



OPEN ACCESS

EDITED BY

Carmen Palomares,
Centro de Investigaciones Energéticas,
Medioambientales y Tecnológicas,
Spain

REVIEWED BY

Uzma Tabassam,
COMSATS University, Islamabad
Campus, Pakistan
Sally Seidel,
University of New Mexico, United States
Hiroshi Okada,
Asia Pacific Center for Theoretical
Physics (APCTP), South Korea

*CORRESPONDENCE

J. Alimena,
juliette.alimena@cern.ch

SPECIALTY SECTION

This article was submitted to Radiation
Detectors and Imaging,
a section of the journal
Frontiers in Physics

RECEIVED 13 June 2022

ACCEPTED 08 August 2022

PUBLISHED 28 September 2022

CITATION

Verhaaren CB, Alimena J, Bauer M,
Azzi P, Ruiz R, Neubert M, Mikulenko O,
Ovchinnikov M, Drewes M, Klaric J,
Blondel A, Rizzi C, Sfyrla A, Sharma T,
Kulkarni S, Thamm A, Blondel A,
Suarez RG and Rygaard L (2022),
Searches for long-lived particles at the
future FCC-ee.
Front. Phys. 10:967881.
doi: 10.3389/fphy.2022.967881

COPYRIGHT

© 2022 Verhaaren, Alimena, Bauer, Azzi,
Ruiz, Neubert, Mikulenko, Ovchinnikov,
Drewes, Klaric, Blondel, Rizzi, Sfyrla,
Sharma, Kulkarni, Thamm, Blondel,
Suarez and Rygaard. This is an open-
access article distributed under the
terms of the [Creative Commons
Attribution License \(CC BY\)](https://creativecommons.org/licenses/by/4.0/). The use,
distribution or reproduction in other
forums is permitted, provided the
original author(s) and the copyright
owner(s) are credited and that the
original publication in this journal is
cited, in accordance with accepted
academic practice. No use, distribution
or reproduction is permitted which does
not comply with these terms.

Searches for long-lived particles at the future FCC-ee

C. B. Verhaaren¹, J. Alimena^{2*}, M. Bauer³, P. Azzi⁴, R. Ruiz⁵,
M. Neubert^{6,7}, O. Mikulenko⁸, M. Ovchinnikov⁸, M. Drewes⁹,
J. Klaric⁹, A. Blondel¹⁰, C. Rizzi¹⁰, A. Sfyrla¹⁰, T. Sharma¹⁰,
S. Kulkarni¹¹, A. Thamm¹², A. Blondel¹³, R. Gonzalez Suarez¹⁴
and L. Rygaard¹⁴

¹Department of Physics and Astronomy, Brigham Young University, Provo, UT, United States, ²Experimental Physics Department, CERN, Geneva, Switzerland, ³Department of Physics, Durham University, Durham, United Kingdom, ⁴INFN, Section of Padova, Padova, Italy, ⁵Institute of Nuclear Physics, Polish Academy of Sciences, Krakow, Poland, ⁶Johannes Gutenberg University, Mainz, Germany, ⁷Cornell University, Ithaca, NY, United States, ⁸Leiden University, Leiden, Netherlands, ⁹Université Catholique de Louvain, Louvain-la-Neuve, Belgium, ¹⁰University of Geneva, Geneva, Switzerland, ¹¹University of Graz, Graz, Austria, ¹²The University of Melbourne, Parkville, VIC, Australia, ¹³LPNHE, Université Paris-Sorbonne, Paris, France, ¹⁴Uppsala University, Uppsala, Sweden

The electron-positron stage of the Future Circular Collider, FCC-ee, is a frontier factory for Higgs, top, electroweak, and flavour physics. It is designed to operate in a 100 km circular tunnel built at CERN, and will serve as the first step towards ≥ 100 TeV proton-proton collisions. In addition to an essential and unique Higgs program, it offers powerful opportunities to discover direct or indirect evidence of physics beyond the Standard Model. Direct searches for long-lived particles at FCC-ee could be particularly fertile in the high-luminosity Z run, where 5×10^{12} Z bosons are anticipated to be produced for the configuration with two interaction points. The high statistics of Higgs bosons, W bosons and top quarks in very clean experimental conditions could offer additional opportunities at other collision energies. Three physics cases producing long-lived signatures at FCC-ee are highlighted and studied in this paper: heavy neutral leptons (HNLs), axion-like particles (ALPs), and exotic decays of the Higgs boson. These searches motivate out-of-the-box optimization of experimental conditions and analysis techniques, which could lead to improvements in other physics searches.

KEYWORDS

future circular collider, particle physics, axion like particles, heavy neutral lepton, Higgs

1 Introduction

The Standard Model (SM) of particle physics is a mature and consistent theory that, after the observation of the Higgs boson, still fails to explain important experimental observations such as dark matter (DM), neutrino masses, or the baryon asymmetry of the Universe (BAU), among others. Theoretical aspects of the SM, including the origins of the electroweak scale, the spectrum of fermions masses, or flavor patterns also await

explanation. These questions may be answered by the direct observation of new particles and phenomena, or by measuring deviations from SM predictions. This is a chief motivation for new colliders that can push both the energy and intensity frontiers.

Long-lived particles (LLPs) are new, beyond the SM (BSM) states that travel a substantial distance between creation and decay in collider systems, presenting distinct experimental signatures [1]. LLPs feature in many BSM models and could provide answers to central questions in particle physics and beyond. The lifetime of a particle depends mostly on its mass and couplings, and so feebly-interacting particles (FIPs), with couplings to the SM particles several orders of magnitude smaller than the SM couplings, are often glaring examples of LLPs.

The experimental signatures of LLPs are particularly interesting. In contrast to promptly decaying particles, LLPs can decay after flying some distance from the primary interaction point. This produces a displaced vertex, with decay products including charged and neutral SM particles (e.g., charged leptons, light neutrinos, and pions). This kind of displaced signature is most commonly associated with LLPs. Other models predict disappearing LLPs giving rise to “short” or “broken” tracks; some are “stopped” or delayed; or produce unusual jets, such as “dark showers.” Such a variety of experimental signatures is very different from the usual SM processes studied at colliders, and any of these signatures would, if observed, constitute a striking “smoking gun” of new physics. In hadron collider environments, standard trigger and reconstruction techniques are often unable to recognize LLP signatures and their study requires dedicated techniques and experiments.

The Future Circular Collider (FCC) program is a design study for a post-LHC particle accelerator at CERN following the priorities set by the 2020 Update of the European Strategy for Particle Physics [2]. The first stage of the FCC design study (FCC-ee) is a high-luminosity, high-precision lepton collider with the goal of better understanding the electroweak (EW) sector, especially the Higgs boson. In addition to a robust program in its own right, FCC-ee will also act as a possible precursor to a high-energy hadron collider (FCC-hh), located in the same tunnel and complementary to it [3].

Though FCC-ee will be a high precision exploration tool, it also opens the possibility of directly discovering new physics [4]. In particular, a future FCC-ee program has an exciting potential for exploring LLPs. The large integrated luminosity of the FCC-ee run around the Z pole, producing 5×10^{12} Z bosons (Tera- Z run), will facilitate direct searches for LLPs that could be closely linked to neutrino masses, explain the BAU, be sound DM candidates, or all at the same time. In the following, three central physics cases are discussed: heavy neutral leptons (HNLs) [5] in the context of the Phenomenological Type I Seesaw model, axion-like particles (ALPs), and exotic Higgs boson decays. In Section 2, the theoretical landscapes of these

three physics cases are outlined. Section 3 discusses the experimental outlook. In particular, the common simulation details (Section 3.1), the experimental aspects of HNLs (Section 3.2), ALPs (Section 3.3), and exotic Higgs boson decays (Section 3.4) at FCC-ee, and considerations for additional detectors for LLPs at FCC-ee (Section 3.5) are covered. Finally, the summary and conclusions are presented in Section 4.

2 Theoretical landscape

In this section, the theoretical frameworks considered are briefly summarized. These representative scenarios are: the Phenomenological Type I Seesaw model (Section 2.1), axion-like particles (Section 2.2), and scalar singlet extensions of the SM (Section 2.3).

2.1 Heavy neutral leptons

The oscillations between neutrino flavor eigenstates in long-baseline experiments [6, 7] is one of the most pressing theoretical puzzles in particle physics today. The neutrino masses that produce these oscillations are also interesting because they imply either the existence of new particles and interactions or substantial changes to the SM paradigm [8, 9].

It is simply not enough to write effective neutrino masses, given the SM’s limited particle content and the desire to understand the mechanism (or mechanisms) that render neutrinos so much lighter than charged leptons and quarks. It is also desirable to understand the flavor/mixing pattern among neutrinos and the possible connections to lepton and quark flavors themselves.

Among the most popular solutions to these mysteries are the Seesaw models. These tie the smallness of neutrino masses (m_{ν_k} with $k = 1, 2, 3$) to the scale of new physics (Λ). Depending on the complexity, the scale (or scales) introduced by these models can range from well below the EW scale to the Planck scale. In the most minimal scenarios [9], general arguments only require Λ to be below 10^{14} GeV. In high-scale Seesaws, light neutrino masses scale inversely with this new physics scale, $m_{\nu_k} \propto 1/\Lambda$. In low-scale Seesaws, the behavior can be more complicated, and in some cases light neutrino masses scale proportionally with this new physics scale, $m_{\nu_k} \propto \Lambda$. The manner in which either is implemented can vary widely, cf. Section 5 in [10], and the most minimal, tree-level constructions are known popularly as the Types I [11–17], II [16, 18–22], and III [23] Seesaw models. Notably, these minimal scenarios are often stepping stones to fuller, more ultraviolet-complete models, including extended gauge theories and grand unified theories. Importantly, neutrino mass models predict a plethora of phenomenology that are testable at a variety of low-

energy and high-energy experiments [10, 24–27], including particle colliders.

A common feature of several popular solutions to the origin of neutrino masses is the hypothetical existence of heavy, sterile neutrinos N_i , or heavy neutral leptons (HNLs) as they are sometimes called. Depending on the precise scenario, they can be Dirac or Majorana fermions, and mediate processes that violate lepton flavor symmetries. In practice, fermions may be arranged in a way that they form a Majorana state with Dirac-like properties [28, 29]. This state is known as a pseudo-Dirac fermion and results from underlying symmetries that explain the smallness of neutrino masses [30–33]. This leads to a phenomenology that practically interpolates between these limiting cases in the sense that the ratio between the rates of the lepton number violating and conserving decays (R_{ll}) can smoothly interpolate between $R_{ll} = 0$ and $R_{ll} = 1$ [34]. Searches for heavy Dirac and Majorana neutrinos at e^+e^- facilities have a long history [35–38], and if they are discovered at the LHC, FCC-ee would be a natural program to study their properties [26, 39–51].

If HNLs mix with the SM neutrinos, they can participate in the SM weak interaction *via* the couplings.

$$\mathcal{L}_{\text{Type I}}^{\text{Int}} = \mathcal{L}^W + \mathcal{L}^Z + \mathcal{L}^H, \quad \text{where} \quad (1a)$$

$$\mathcal{L}^W = -\frac{g_W}{\sqrt{2}} \sum_{\ell=e}^{\tau} \sum_{i=1}^{n_s} \bar{N}_i V_{\ell i}^* W_{\mu}^+ \gamma^{\mu} P_L \ell + \text{H.c.}, \quad (1b)$$

$$\mathcal{L}^Z = -\frac{g_W}{2 \cos \theta_W} \sum_{\ell=e}^{\tau} \sum_{i=1}^{n_s} \bar{N}_i V_{\ell i}^* Z_{\mu} \gamma^{\mu} P_L \nu_{\ell} + \text{H.c.}, \quad (1c)$$

$$\mathcal{L}^H = -\frac{g_W}{2M_W} h \sum_{\ell=e}^{\tau} \sum_{i=1}^{n_s} \bar{N}_i V_{\ell i}^* m_{N_i} P_L \nu_{\ell} + \text{H.c.} \quad (1d)$$

Here, N_1, \dots, N_{n_s} are the heavy mass eigenstates of the theory. This model (1) is a common HNL benchmark for the pure type I Seesaw we use in this study. In extended models, the HNLs may have extra interactions, such as new gauge interactions [52–60]. The number of right-handed neutrino chiral eigenstates n_s is not constrained by gauge anomaly considerations in the model (1) because the chiral states are gauge singlets. Here, the $V_{\ell N_i}$ are the complex-valued, active-sterile mixing matrix elements and describe the coupling between the heavy mass eigenstate i and lepton flavor state ℓ .

The Lagrangian (1) approximates interactions to first order in the parameter $|V_{\ell i}|$. In this phenomenological framework, the masses of N_i (m_{N_i}) and $V_{\ell i}$ are taken to be independent. Hypothesizing connections to other physics, e.g., the relic abundance of DM or the matter-antimatter asymmetry of the observable Universe, can greatly constrain masses and mixing, cf. Section 2.1.2. For simplicity, the analysis of Section 3.2 considers only the lightest heavy mass eigenstate N_1 , denoted by N , with mass and mixing m_N and $V_{\ell N}$. It is important to stress that considering only one HNL is for bench-marking and discovery

purposes; realistic scenarios usually contain multiple mass eigenstates.

In analogy to the SM effective field theory (SMEFT) framework [61–63], the above Lagrangian can be systematically extended by higher dimensional operators in a framework known as ν SMEFT [64–66], which can parameterize ultraviolet completions.

In the minimal Type I Seesaw model, where $n_s = 2$, the requirement to reproduce the observed pattern of light neutrino masses and mixing imposes testable constraints on the relative size of the HNL couplings $|V_{\ell i}|^2$ to individual SM flavors [67–70]. These will improve in the future with the Deep Underground Neutrino Experiment (DUNE) [71], cf. Figure 1, leading to a prediction that can be tested with FCC-ee. The position in the triangle in Figure 1 is entirely determined by the low energy phases in the Pontecorvo-Maki-Nakagawa-Sakata (PMNS) matrix. The number of events observed in displaced decays of HNLs produced during the Z pole run permits the determination of the relative mixing $|V_{\ell i}|^2/(\sum_{\ell} |V_{\ell i}|^2)$ at the percent level [44], allowing for the Majorana phase in the light neutrino mixing matrix to be indirectly constrained [68, 72]. For $n_s = 3$, the model is less constrained, and making a testable prediction would require an independent determination of the lightest neutrino mass in the SM, cf. Figure 11 in [70]. Beyond minimal models, measuring the $|V_{\ell i}|^2/(\sum_{\ell} |V_{\ell i}|^2)$ can give insight into flavor at charge-parity (CP) symmetries of the neutrino mixing matrix [73–75], providing a hint towards possible ultraviolet completions.

2.1.1 Phenomenology of Dirac and Majorana heavy neutral leptons

In the kinematically accessible regime, FCC-ee is an excellent machine to discover HNLs [39] and study their properties. An analysis was completed for prompt HNL signals [79] and reproduced in Ref. [3]. A comparison for various machines and setups was compiled for the European Strategy for Particle Physics Briefing Book [80]¹. The sensitivity to active-sterile mixing, labeled here by Θ , is shown in the summary figure, Figure 2. Figure 3 shows an updated estimation of different sensitivities for current and proposed detectors including an FCC-ee displaced vertex analysis.

Figure 4 shows the four and one event contours. The four event contour corresponds to the 95% confidence level (CL) exclusion in the absence of signal events. The one event contour shows that for the analysis of the LLP signatures, there still is a 63% probability to observe one event, which, in the absence of background events, could be sufficient for discovery, all the way down to the see-saw limit around 20–40 GeV.

If N is a Majorana fermion, then it can mediate processes that conserve lepton number as well as those that violate lepton

¹ Figure 8.19.

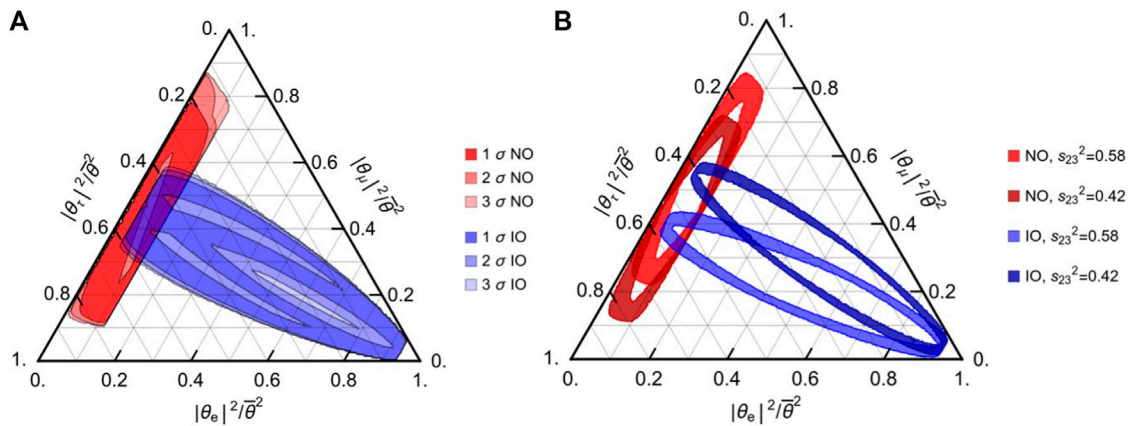


FIGURE 1
 Allowed range for the relative magnitude of the HNL couplings to individual SM flavors in the model (27) with $n_s = 2$, plot taken from [5]. **(A):** The range of relative flavor mixings $(\sum_i |V_{ei}|^2)/(\sum_{i,j} |V_{ei}|^2)$ consistent with the current neutrino oscillation data, cf. e.g., [68, 69, 76]. The contours correspond to the allowed $\Delta\chi^2$ range taken from [77] for the case of normal (red) and inverted (blue) light neutrino mass ordering. **(B):** The projected 90% CL contours for the relative mixings after 14 years of data taking at DUNE [78], assuming maximal CP violation $\delta = -\pi/2$ and two benchmark values of the PMNS angle θ_{23} , taken from the DUNE TDR [71], as indicated in the legend. FCC-ee can measure these ratios to the percent level in displaced HNL decays [44].

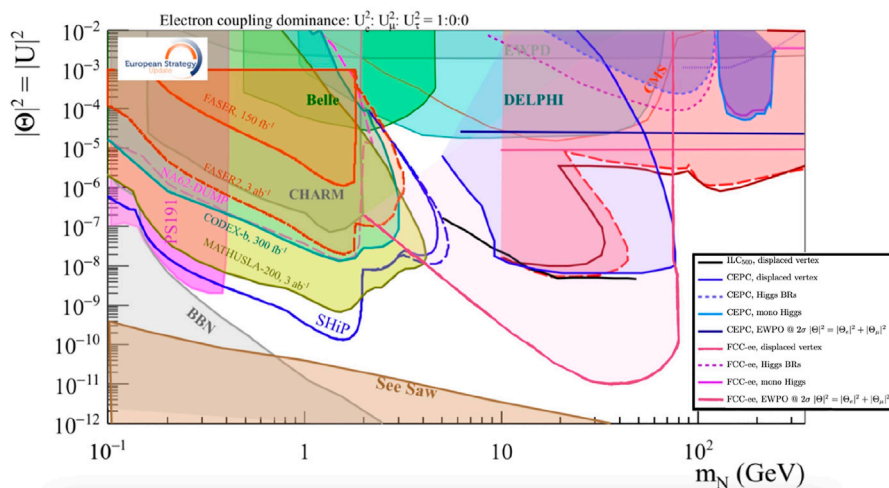
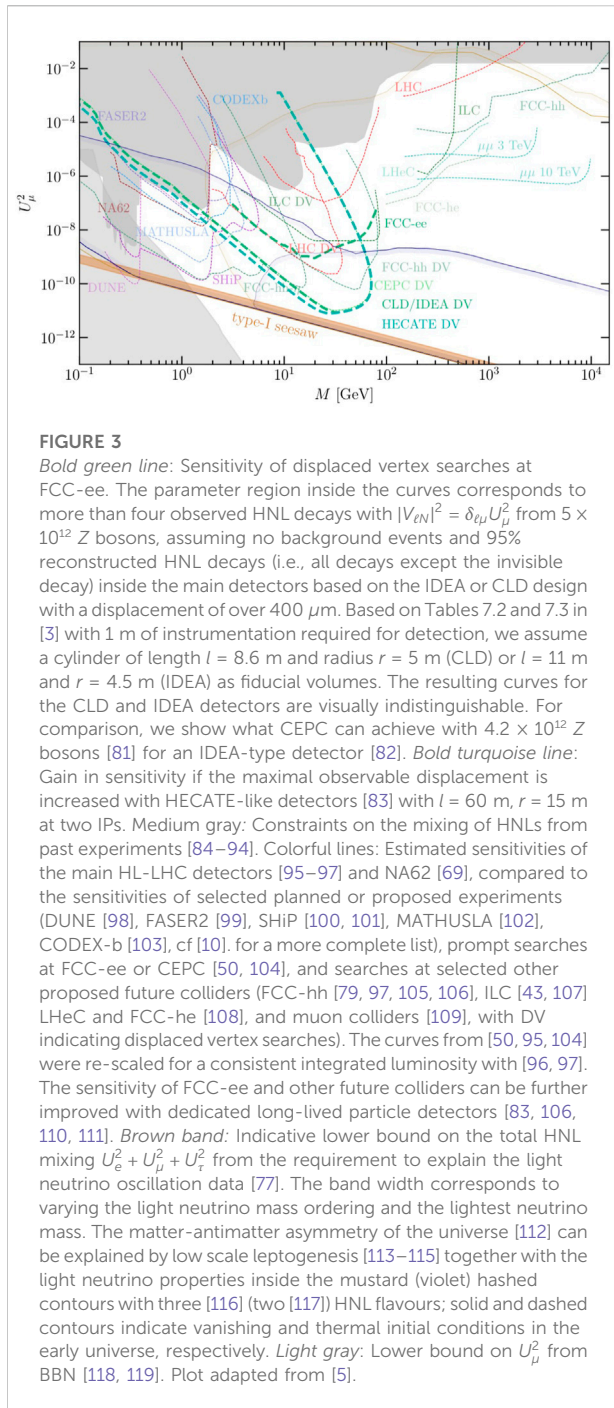


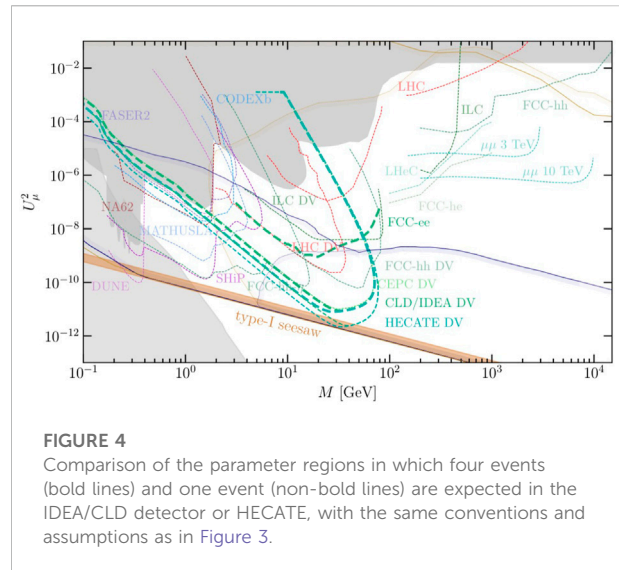
FIGURE 2
 90% CL exclusion limits for a Heavy Neutral Lepton mixed with the electron neutrino, as presented in the European Strategy for Particle Physics Briefing Book [80]. The FCC-ee curves are in (overlined) dark purple—for FCC-ee, this is equivalent to a plot as function of the sum of matrix elements squared $|U_N|^2$. The curve below the Z boson mass corresponds to the combined LLP and prompt analysis performed with $10^{12}Z$ in Ref. [79]. The horizontal limit at high masses results from the effect of light-heavy neutrino mixing on the EW precision observables and remains valid up to $O(1000 \text{ TeV})$.

number. Likewise, if lepton number is violated, then neutrinos must in principle possess Majorana properties [120, 121], though the amount of lepton number violation (LNV) in practice depends on the underlying model [121, 122]. Dirac neutrinos can only participate in processes that conserve lepton number. Therefore, differences between Dirac and Majorana N are closely

related to differences between lepton number conservation (LNC) and LNV. The availability of LNV decay modes, for instance, leads to a Majorana N having a width (Γ_N) that is twice as large as a Dirac N . This implies that a Majorana N has a mean lifetime (τ_N), or mean displacement (d_N), that is half as long as that of a Dirac N .



Section 3.2.3 assumes a simple phenomenological model (1) with $n_s = 1$, i.e., only one mass eigenstate N that is either a Dirac or a Majorana fermion. Though this phenomenological model cannot completely reproduce the light neutrino oscillation data, it is sufficient to capture the collider phenomenology of the pure Dirac and Majorana HNLs benchmarks experimentally. Nature may be somewhere in the middle of these two cases. Therefore, observables that



quantify differences between LNV and LNC processes, such as $R_{\ell\ell}$ as defined in [34] or \mathcal{A} as defined in [123, 124], can be used to interpolate between the benchmarks.

There is a rich phenomenology that connects $R_{\ell\ell}$, \mathcal{A} , and the decay rates of HNLs into different SM flavors to the mechanism that generates light neutrino masses. This connection can be accurately probed by studying the HNL properties at FCC [37, 48, 125] or other colliders [34, 123, 124, 126].

2.1.2 Probing cosmological questions

In addition to generating light neutrino masses, HNLs can, depending on their mass, affect the history of the Universe in different ways [114, 127, 128]. From a cosmological viewpoint, the most important motivation for HNL searches may be their potential connection to the origins of baryonic matter and DM.

Leptogenesis: Leptogenesis [129] provides an explanation for the matter-antimatter asymmetry in the observable Universe [112] and relates it to the properties of neutrinos. In the most popular scenario (based on the Type I Seesaw), HNLs generate the BAU *via* their CP-violating interactions with the thermal plasma. While it was originally believed that this mechanism only operates for HNL masses far above the EW scale [130], it is now established that sub-TeV HNLs can produce the observed BAU during their production [113, 114, 127] or freeze-out and decay [115, 131]. This implies that direct experimental searches have the potential to probe the origin of matter [132]. If any HNLs with masses at or below the EW scale are discovered in the near future, FCC-ee would provide a powerful tool to study their properties and test their connection to the BAU. A simple construction that supports low-scale leptogenesis is the Neutrino Minimal Standard Model (νMSM) [127]. Here, two HNLs simultaneously explain the neutrino masses and the BAU [114] for a wide range of experimentally accessible masses, cf.

Figure 3. Due to its minimality, the model is highly testable [67, 68]. In particular, leptogenesis constrains the flavor mixing pattern beyond the experimental fits shown in Figure 1, which can be tested by comparing flavored branching ratios in displaced decays. Finally, if accessible, HNL oscillations in the detectors are sensitive to the HNL mass splitting [44], which is a crucial parameter for leptogenesis.

Dark matter: HNLs with sufficiently small masses and mixing angles could be viable DM candidates [133]. Constraints on the HNL lifetime and from indirect searches restrict the range of masses and mixings to values that are inaccessible to direct searches at colliders, cf [134, 135]. for reviews. However, FCC-ee can indirectly probe sterile neutrino SM scenarios by searching for signatures of other particles that were involved in the DM production.

HNLs can be resonantly produced in the early Universe through their mixing-suppressed weak interactions if the lepton asymmetry at temperatures around the quantum chromodynamics (QCD) crossover greatly exceeded the BAU [136–139]. In the ν MSM, this large lepton asymmetry can be generated by heavier HNLs that are also responsible for the BAU and neutrino masses [140]. The first parameter space studies [141–143] suggest that this is possible only for comparably small mixing angles, possibly making FCC-ee or a similar machine the only facility at which these HNLs could be discovered. If the HNLs have additional gauge interactions (cf. e.g., [144–149]), the extended gauge sector can be probed directly or indirectly at FCC-ee. If the DM is produced via the decay of a singlet [150–152] or charged [153, 154] scalar during freeze-out or freeze-in [155, 156], precision studies of the SM Higgs and of the portal can shed light on the mechanism. Most of these possibilities have not been studied in detail to date.

2.2 Axion-like particles

Many models that address open, fundamental problems of the SM are governed by global symmetries. If an approximate global symmetry is spontaneously broken, a pseudo Nambu-Goldstone boson appears in the theory that is light compared to the symmetry breaking scale. If this pseudo Nambu-Goldstone boson is a pseudoscalar, it is often referred to as an axion-like particle or ALP. The ALP’s lightness singles it out as a uniquely promising experimental target that could open a first window onto high-scale new physics beyond the SM.

ALPs appear in many models that address open, fundamental problems in the SM. The most prominent example is the QCD axion, which was introduced in the 1980s to solve the strong CP problem [157–160] and found to simultaneously account for the observed DM relic abundance [161, 162]. QCD axions are typically very light, and these models are plagued by the “axion quality”

problem, in which quantum gravity corrections destabilize the minimum of the axion potential, thereby reintroducing the strong CP problem [163–166]. Heavy-axion solutions to the strong CP problem circumvent this issue and so motivate ALPs with MeV-to-TeV scale masses [167–175]. ALPs in this mass range could also result from the breaking of global symmetries in low scale supersymmetric [176–178] or composite Higgs models [179–182]. Phenomenologically, they can also lead to successful EW baryogenesis [183].

An ALP dominantly couples to SM particles *via* dimension-5 operators,

$$\begin{aligned} \mathcal{L}_{\text{eff}} = & \frac{1}{2}(\partial_\mu a)(\partial^\mu a) - \frac{m_{a,0}^2}{2} a^2 + \sum_\psi \frac{c_{ff}}{2} \frac{\partial^\mu a}{f} \bar{\psi} \gamma_\mu \gamma_5 \psi \\ & + c_{GG} \frac{\alpha_s}{4\pi} \frac{a}{f} G_{\mu\nu}^a \tilde{G}^{\mu\nu,a} + c_{\gamma\gamma} \frac{\alpha}{4\pi} \frac{a}{f} F_{\mu\nu} \tilde{F}^{\mu\nu} \\ & + c_{\gamma Z} \frac{\alpha}{2\pi s_w} \frac{a}{f} F_{\mu\nu} \tilde{Z}^{\mu\nu} + c_{ZZ} \frac{\alpha}{4\pi s_w^2} \frac{a}{f} Z_{\mu\nu} \tilde{Z}^{\mu\nu} \\ & + c_{WW} \frac{\alpha}{2\pi s_w^2} \frac{a}{f} W_{\mu\nu}^+ \tilde{W}^{-\mu\nu}, \end{aligned} \tag{2}$$

where $G_{\mu\nu}^a$ is the field-strength tensor of $SU(3)_c$, while $F_{\mu\nu}$, $Z_{\mu\nu}$ and $W_{\mu\nu}^+$ describe the photon, Z, and W boson in the broken phase of EW symmetry. The dual field-strength tensors are denoted by $\tilde{F}^{\mu\nu} = \frac{1}{2}\epsilon^{\mu\nu\alpha\beta} F_{\alpha\beta}$, etc., (with $\epsilon^{0123} = 1$); α_s and α are the QCD coupling and fine-structure constants, respectively; s_w and c_w denote the sine and cosine of the weak mixing angle; and the sum runs over all fermion mass eigenstates ψ . The suppression scale f is related to the new physics scale Λ via $\Lambda = 4\pi f$, and to the axion decay constant f_a by $f_a = -f/(2c_{GG})$. The ALP dominantly interacts with the Higgs boson *via* dimension-6 and -7 operators,

$$\mathcal{L}_{\text{eff}}^H = \frac{c_{ah}}{f^2} (\partial_\mu a)(\partial^\mu a) H^\dagger H + \frac{c_{Zh}}{f^3} (\partial^\mu a)(H^\dagger iD_\mu H + \text{h.c.}) H^\dagger H. \tag{3}$$

At FCC-ee, ALPs are predominantly produced in association with a photon, Z boson, or Higgs boson, as shown in the Feynman diagrams in Figure 5, or *via* exotic Z and Higgs decays. Resonant production of an ALP, e.g., $e^+e^- \rightarrow a$, is possible but suppressed by $m_e^2/(4\pi f)^2$. ALP production in vector boson fusion has been considered in Ref. [184] and detection prospects in light-by-light scattering in Refs. [185, 186].

The differential cross sections for associated $\gamma a/Za/ha$ production are given by [187, 188].

$$\begin{aligned} \frac{d\sigma(e^+e^- \rightarrow \gamma a)}{d\Omega} = & \frac{\alpha\alpha^2(s)}{128\pi^3} \frac{s^2}{f^2} \left(1 - \frac{m_a^2}{s}\right)^3 (1 + \cos^2\theta) \\ & \times (|V_\gamma(s)|^2 + |A_\gamma(s)|^2), \end{aligned} \tag{4}$$

$$\begin{aligned} \frac{d\sigma(e^+e^- \rightarrow Za)}{d\Omega} = & \frac{\alpha\alpha^2(s)}{128\pi^3} \frac{s^2}{f^2} \lambda^{\frac{1}{2}}(x_a, x_Z) (1 + \cos^2\theta) \\ & \times (|V_Z(s)|^2 + |A_Z(s)|^2), \end{aligned} \tag{5}$$

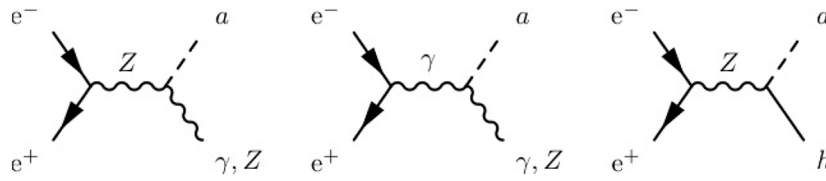


FIGURE 5
ALP production processes in electron-positron collisions.

$$\frac{d\sigma(e^+e^- \rightarrow ha)}{d\Omega} = \frac{2\pi^3 \alpha |c_{Zh}|^2}{c_w^2 s_w^2} \frac{s m_Z^2}{f^2 (s - m_Z^2)^2} \lambda^{\frac{3}{2}}(x_a, x_h) \sin^2 \theta (g_V^2 + g_A^2), \quad (6)$$

where $\lambda(x, y) = (1 - x - y)^2 - 4xy$, $x_i = (m_i^2/s)$, \sqrt{s} is the center-of-mass energy, and θ describes the scattering angle of the photon, Z, or Higgs boson relative to the beam axis. The vector and axial-vector form factors are given by

$$V_y(s) = \frac{c_{\gamma\gamma}}{s} + \frac{g_V}{2c_w^2 s_w^2} \frac{c_{yZ}}{s - m_Z^2 + im_Z \Gamma_Z}, \quad (7)$$

$$A_y(s) = \frac{g_A}{2c_w^2 s_w^2} \frac{c_{yZ}}{s - m_Z^2 + im_Z \Gamma_Z},$$

$$V_Z(s) = \frac{1}{c_w s_w} \frac{c_{yZ}}{s} + \frac{g_V}{2c_w^3 s_w^3} \frac{c_{ZZ}}{s - m_Z^2 + im_Z \Gamma_Z}, \quad (8)$$

$$A_Z(s) = \frac{g_A}{2c_w^3 s_w^3} \frac{c_{ZZ}}{s - m_Z^2 + im_Z \Gamma_Z},$$

with $g_V = 2s_w^2 - 1/2$, $g_A = -1/2$, and Γ_Z is the total width of the Z boson. The process where an ALP is radiated off an initial-state electron exhibits an additional suppression of (m_e^2/s) .

The integrated cross section of $e^+e^- \rightarrow \gamma a$ below the Z pole is dominated by the photon contribution, which is proportional to $c_{\gamma\gamma}$, while above the Z pole the process proportional to c_{yZ} also contributes. Combining these measurements at low and high energies therefore enables us to access these couplings separately. At the Z pole, the cross section becomes

$$\sigma(e^+e^- \rightarrow \gamma a) \approx \frac{\alpha}{24\pi^2} \alpha^2 (m_Z^2) \left(1 - \frac{m_a^2}{m_Z^2}\right)^3 \left[\frac{|c_{\gamma\gamma}|^2}{f^2} + \frac{m_Z^2}{\Gamma_Z^2} \frac{|c_{yZ}|^2}{16s_w^4 c_w^4 f^2} \right]. \quad (9)$$

The contribution from the Z boson propagator is enhanced by $(m_Z^2/\Gamma_Z^2) \sim 1336$, which allows one to directly access the coupling c_{yZ} (as long as $c_{\gamma\gamma}$ is not much bigger than c_{yZ}). ALPs can also be produced in exotic decays of Z and Higgs bosons [187–189]. The exotic decay rates are given by

$$\Gamma(Z \rightarrow \gamma a) = \frac{\alpha \alpha (m_Z) m_Z^3}{96\pi^3 s_w^3 c_w^2 f^2} |c_{yZ}|^2 \left(1 - \frac{m_a^2}{m_Z^2}\right)^3, \quad (10)$$

$$\Gamma(h \rightarrow Za) = \frac{m_h^3 v^2}{64\pi f^6} |c_{Zh}|^2 \lambda^{3/2} \left(\frac{m_Z^2}{m_h^2}, \frac{m_a^2}{m_h^2}\right), \quad (11)$$

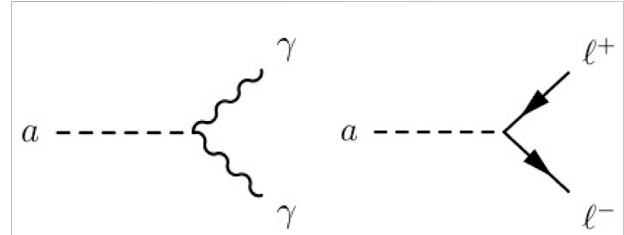


FIGURE 6
ALP decay processes at FCC-ee.

$$\Gamma(h \rightarrow aa) = \frac{m_h^3 v^2}{32\pi f^4} |c_{ah}|^2 \left(1 - \frac{2m_a^2}{m_h^2}\right)^2 \sqrt{1 - \frac{4m_a^2}{m_h^2}}. \quad (12)$$

Once produced, ALPs lead to a variety of signatures inside the detector. Very long-lived ALPs, for example, escape the detector and lead to a signature with missing momentum. ALPs with somewhat shorter lifetimes may decay into gauge bosons, leptons, and quarks inside the detector. The photon and lepton decay channels are shown in Figure 6. Their corresponding decay widths are given by

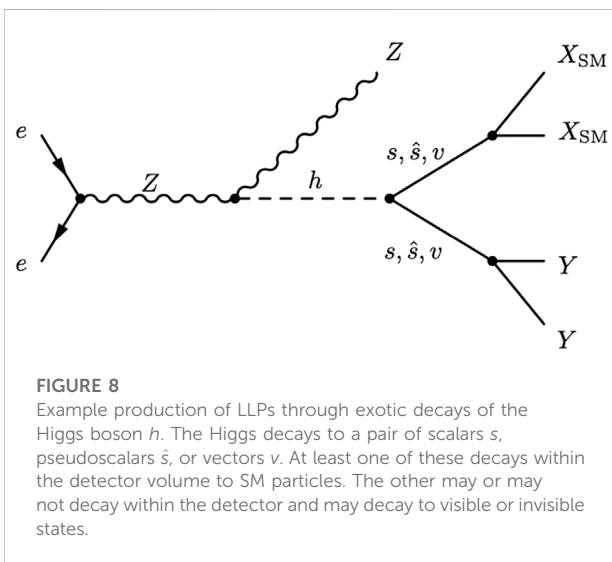
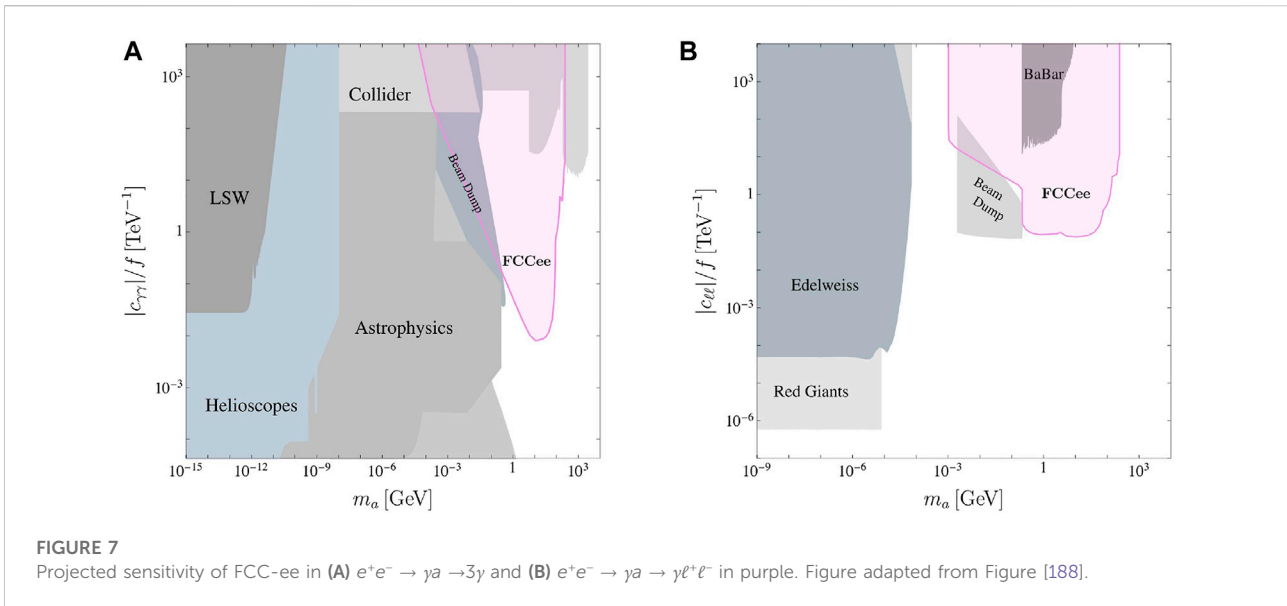
$$\Gamma(a \rightarrow \gamma\gamma) = \frac{\alpha^2 m_a^3}{64\pi^3 f^2} c_{\gamma\gamma}^2, \quad (13)$$

$$\Gamma(a \rightarrow \ell^+ \ell^-) = \frac{m_a m_\ell^2}{8\pi f^2} c_{\ell\ell}^2 \sqrt{1 - \frac{4m_\ell^2}{m_a^2}}. \quad (14)$$

An ALP decay into hadrons can be computed perturbatively for relatively large ALP masses, i.e., $m_a \gg \Lambda_{\text{QCD}}$. The decay width into bottom quarks specifically is given by

$$\Gamma(a \rightarrow b\bar{b}) = \frac{3 m_a m_b^2(m_a)}{8\pi f^2} c_{bb}^2 \sqrt{1 - \frac{4m_b^2}{m_a^2}}, \quad (15)$$

and similarly for $\Gamma(a \rightarrow c\bar{c})$. The decay rate into light quarks (u, d, s) can be computed using quark-hadron duality and is given by [187, 190].



$$\Gamma(a \rightarrow \text{light hadrons}) = \frac{\alpha_s^2(m_a) m_a^3}{8\pi^3 f^2} \left[1 + \frac{83}{4} \frac{\alpha_s(m_a)}{\pi} \right] |C_{GG}^{\text{eff}}(m_a)|^2, \tag{16}$$

where the ALP couplings to both gluons and quarks contribute via

$$C_{GG}^{\text{eff}}(m_a) = c_{GG} + \frac{1}{2} \sum_{q \neq t} c_{qq} B_1 \left(\frac{4m_q^2}{m_a^2} \right). \tag{17}$$

The function B_1 behaves as $B_1(4m_q^2/m_a^2) \approx 1$ for $m_q \ll m_a$ and $B_1(4m_q^2/m_a^2) \approx -m_a^2/(12m_q^2)$ for $m_q \gg m_a$. The explicit form of B_1 is given in e.g., [187]. For light ALPs, $m_a \ll \Lambda_{\text{QCD}}$, the decay into three pions may be kinematically accessible, with a decay

rate which is given in [187, 191]. However, it is worth noting that the FCC-ee program as currently envisioned will not be able to produce significant numbers of ALPs that are heavy enough to decay in two top quarks, due to the high center of mass energy that would be required. Depending on their lifetime, ALPs can decay promptly at the interaction point or they may decay after having travelled a certain distance inside the detector.

At FCC-ee, all combinations of ALP production modes with visible and invisible decay modes can be investigated [188, 192]. While many processes, in particular exotic Higgs decays, depend on two independent couplings, under certain assumptions a few processes only depend on a single coupling parameter. For example, the $e^+e^- \rightarrow \gamma a \rightarrow 3\gamma$ and $e^+e^- \rightarrow Z a \rightarrow Z\gamma\gamma$ processes only depend on the ALP-photon coupling $c_{\gamma\gamma}$ when it is assumed that both the ALP-photon and the ALP-photon-Z couplings originate from the ALP coupling to either $SU(2)_L$ or $U(1)$ gauge bosons before EW symmetry breaking. If the ALP only couples to $U(1)$ gauge bosons, then $c_{\gamma Z} = -s_w^2 c_{\gamma\gamma}$. In this case, Figure 7A shows the projected sensitivity of FCC-ee to $c_{\gamma\gamma}$ using the $e^+e^- \rightarrow \gamma a \rightarrow 3\gamma$ channel [188]. This analysis assumes at least four signal events and combines the Z-pole run with runs at $\sqrt{s} = 2m_W$ and $\sqrt{s} = 250$ GeV. Further details are provided in [188]. Another process that depends only on a single coupling is $e^+e^- \rightarrow \gamma a \rightarrow \gamma \ell^+ \ell^-$ when the ALP-photon and the ALP-photon-Z couplings are induced via a loop of leptons. In this case,

$$c_{\gamma\gamma} = \sum_{\ell=e,\mu,\tau} c_{\ell\ell} B_1(4m_\ell^2/m_a^2) \quad \text{and} \quad c_{\gamma Z} = (s_w^2 - 1/4)c_{\gamma\gamma}. \tag{18}$$

Figure 7B shows the projected sensitivity of FCC-ee to $c_{\ell\ell}$ using the process $e^+e^- \rightarrow \gamma a \rightarrow \gamma \ell^+ \ell^-$ [188].

The $e^+e^- \rightarrow \gamma a \rightarrow 3\gamma$ and $e^+e^- \rightarrow \gamma a \rightarrow \gamma \ell^+ \ell^-$ searches are sensitive to ALP decay lengths of up to 1.5 m and 2 cm, respectively. The search for long-lived ALPs may be significantly improved with the installation of a dedicated far detector that could probe decay lengths of up to 100 m [193, 194]. For FCC-ee reach on the relaxation, see Ref. [195]. In addition to direct measurements, FCC-ee will be able to significantly constrain the ALP contribution to the oblique parameters [187, 188], whose determination is expected to improve by an order of magnitude [196].

2.3 Exotic Higgs boson decays

The Higgs boson has a unique role within the SM. It is the only apparently elementary scalar particle that has been discovered. In particular, whatever new physics is responsible for the cosmological DM, the apparent asymmetry between matter and antimatter, or small neutrino masses may well have some coupling to the Higgs boson. In short, the Higgs boson is a likely gateway to what lies beyond the SM.

The two-body decays of the Higgs boson to SM particles are controlled by small Yukawa couplings or loop suppression making its decay width much smaller than its mass. Consequently, current bounds on the Higgs width leave plenty of room for “exotic” decays, that is, decays not predicted by the SM. However, future colliders, like FCC-ee, will be able to measure the Higgs width much more precisely than at the LHC [197]. The products of these exotic Higgs boson decays can decay promptly themselves or be completely stable, each of which present their own experimental challenges and advantages. However, searches for particles whose lifetimes are more intermediate, i.e., that decay within the experimental detector but at a measurable distance from the interaction point, can have very low backgrounds in comparison to prompt searches. This gives Higgs boson decays to LLPs remarkable power to probe particles and sectors whose couplings to the Higgs are small but nonzero. The e^+e^- to Zh processes shown in Figure 8 illustrate the utility of the FCC-ee collider. Because the initial state and the Z decays are well understood, invisible, partially invisible, and displaced decays of the Higgs boson can be probed with confidence. For a review, see Ref. [102] and the recent work in Ref. [198].

The characteristics of LLPs vary considerably. Exotic Higgs decays to spin-zero particles are considered first. Such decays at future lepton colliders were considered in Ref. [199]. Long-lived scalars may result from simple constructions, such as adding a single scalar field to the SM:

$$V_{\text{scalar}} = V_H + V_S + c_1 S |H|^2 + c_2 S^2 |H|^2. \quad (19)$$

They may also arise in rich, hidden sectors such as Hidden Valley models [200–202]. Of particular interest are hidden sectors motivated by Neutral Naturalness [203–206]. These models address the little hierarchy problem through new symmetries,

but the symmetry partners of the SM quarks do not carry SM color. Instead they are charged under a hidden, QCD-like confining force.

In many models with the long-lived scalar s or pseudoscalar \hat{s} , the Higgs boson decay products inherit much of the Higgs’ coupling structure. While the actual size of the couplings are reduced by a common small mixing angle θ , the branching fractions are those of a SM Higgs boson with the mass of the LLP. In the scalar case, one often finds

$$\Gamma(s \rightarrow X_{\text{SM}} X_{\text{SM}}) = \sin^2 \theta \Gamma(h(m_s) \rightarrow X_{\text{SM}} X_{\text{SM}}). \quad (20)$$

The pseudoscalar case is slightly modified [207–209] and can also include the $h \rightarrow \hat{s} Z$ decay channel, see for instance the ALP results given in Eqs 11, 12. Since the masses of the LLPs must be less than half the Higgs boson mass, the dominant decays modes are into the heaviest kinetically accessible SM quarks. Thus, for Higgs boson decays into spin-zero LLPs, hadronic final states, and b -jets especially, are particularly motivated.

Rather than scalars, the LLPs may be spin-half fermions. These can be related to the BAU [210] or to Seesaw explanations of the neutrino masses [11–17]. The heavy neutrinos N in these models have been shown to have a wide range of possible decay lengths, including within the volume of an FCC-ee detector [211–213]. The N mainly decay into a SM lepton and an off-shell weak gauge boson. This leads to three-body final states which may be composed of both quarks (jets) and leptons.

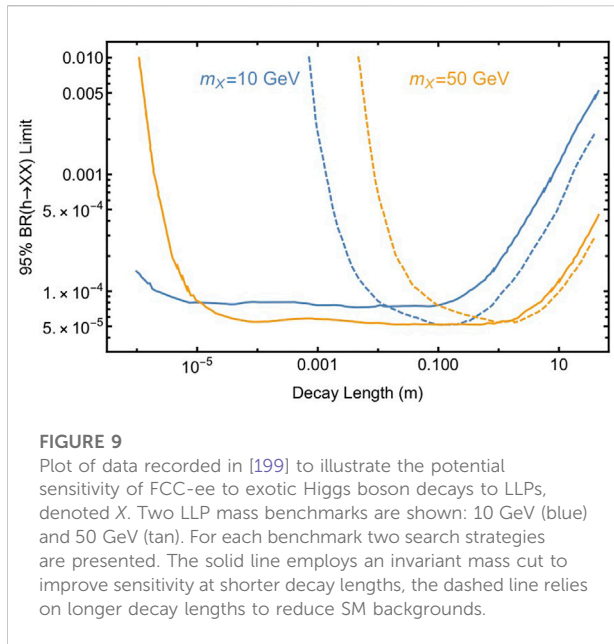
The Higgs boson can also decay to long-lived vectors v . A simple framework is the Hidden Abelian Higgs model [214]. In this case, a new $U(1)'$ gauge symmetry is broken by a hidden Higgs field h_D that generates a vacuum expectation value (VEV). The hidden photon A'_μ of the new gauge symmetry gets a mass proportional to the hidden Higgs VEV and can also have kinetic mixing with the SM through

$$-\frac{\epsilon}{2 \cos \theta_W} F'_{\mu\nu} F_Y^{\mu\nu}, \quad (21)$$

where θ_W is the weak mixing angle and $F_Y^{\mu\nu}$ is the field strength for SM hypercharge. The parameter ϵ can vary over a huge range, and controls the degree to which SM fermions couple to A'_μ . For sufficiently small ϵ , the massive hidden photon is a LLP.

The hidden photon’s coupling to SM fields is proportional to their hypercharge. This means that, when and if they are kinematically accessible, quark final states make up most of its branching fraction, though decay rates to leptons are non-negligible. A small ϵ also means that the direct coupling of the hidden photon to the SM Higgs boson is small. However, the mixing between SM Higgs and the hidden Higgs can be larger than ϵ . This allows the Higgs boson to decay to two hidden photons at a larger rate.

In summary, the Higgs boson may have appreciable decay widths into LLPs of various spin. The decay modes of the LLPs can vary, but it has been shown that hadronic final states play a significant role in all the decay types outlined above. Decays to



long-lived fermions stand out as different, in that their leading decays are three-body. Pseudoscalars may also lead to $h \rightarrow \hat{s}Z$ decays, but in general, the $h \rightarrow XX$ process captures most of the interesting possibilities. Assuming the X particle has significant branching into SM quarks (and possibly into b quarks in particular) appears to be the most motivated benchmark. Of course, the variety of other decays can be leveraged in more model-specific analyses.

Figure 9 displays an illustration, taken from Ref. [199], of how sensitive FCC-ee can be to Higgs boson decays to long-lived X particles. The 95% limit on the exotic branching fraction to these particles is plotted as a function of the X 's decay length. Two mass benchmarks, $m_X = 10$ (blue) and 50 (tan) GeV, are shown (additional benchmarks are considered in Ref. [199]) for two search strategies. The solid line corresponds to using an invariant mass cut to retain sensitivity to shorter decay lengths. In contrast, the dashed line depends on longer decay lengths to reduce SM backgrounds.

3 Experimental outlook

This section presents new studies produced for this paper that follow up on the theoretical landscape presented in Section 2.

3.1 Simulation details

For all signal and background processes, the event generator MadGraph5_aMC@NLO v3.2.0 [215, 216] is used to simulate at

leading order unpolarized, parton-level e^+e^- collisions at $\sqrt{s} = 91$ GeV. For all processes, parton-level events are passed to Pythia [217] v8.303 to simulate parton showering and hadronization. For each signal benchmark point, 50×10^3 unscaled events were generated, and for each background process, 10^7 – 10^9 unscaled events were generated, depending on the process.

The detector response is simulated with Delphes v3.4.2 [218], using the latest Innovative Detector for Electron-positron Accelerators (IDEA) FCC-ee detector concept [219] card. The IDEA detector comprises of a silicon pixel vertex detector; a large-volume, light short-drift wire chamber surrounded by a layer of silicon micro-strip detectors; a thin, low-mass superconducting solenoid coil; a pre-shower detector; a dual-readout calorimeter; and muon chambers within the magnet return yoke.

The k4SimDelphes project [220] converts Delphes objects to the EDM4HEP format [221], which is the common data format used for the simulation of future colliders. A sophisticated analysis framework has been developed for all FCC analyses using the EDM4hep format. It is based on RDataFrames [222], where C++ code is compiled in a ROOT [223] dictionary as “analysers.” These are subsequently called in Python. Several external packages, such as ACTS [224], FastJet [225], and awkward [226], are included.

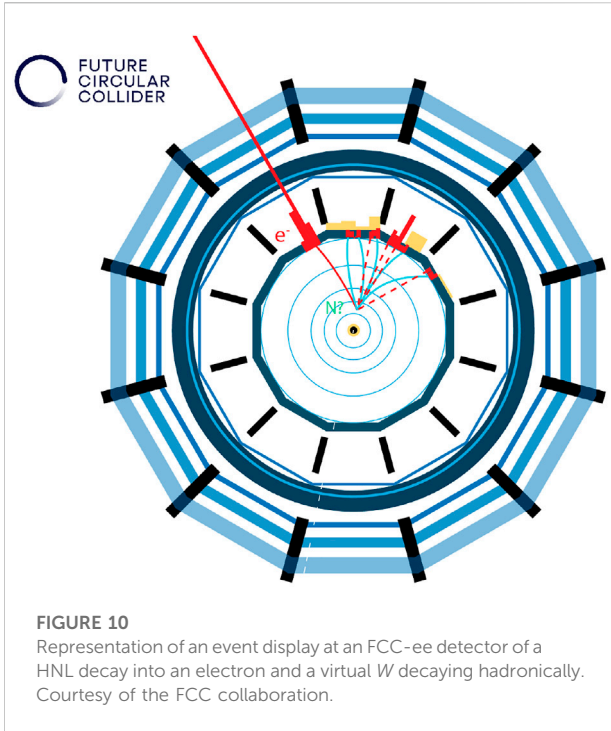
3.1.1 Heavy neutral leptons

To study Dirac and Majorana HNLs at FCC-ee, the processes.

$$\text{Majorana } N: e^+e^- \rightarrow Z \rightarrow N\nu_e + N\bar{\nu}_e, \quad \text{with } N \rightarrow e^+e^-\nu_e + e^+e^-\bar{\nu}_e, \quad (22a)$$

$$\text{Dirac } N: e^+e^- \rightarrow Z \rightarrow N\bar{\nu}_e + \bar{N}\nu_e, \quad \text{with } N (\bar{N}) \rightarrow e^+e^-\nu_e (\bar{\nu}_e), \quad (22b)$$

are simulated using the HeavyN [227, 228] and HeavyN_Dirac [97, 228] universal FeynRules Object [229–231] libraries in conjunction with MadGraph5_aMC@NLO. These libraries implement the interaction Lagrangian described in Section 2.1 for Majorana and Dirac N , respectively. A representative subset of Feynman diagrams common to both the Dirac and Majorana case is shown in Figure 11. For the Majorana case, both LNC and LNV channels are included. The Dirac case only permits LNC channels. The preservation of spin correlation in the production and decay of N with this setup was checked in Ref. [124]. When unspecified, the results consider the Majorana case. As a further benchmark, the assumption that N couples only to the electron-flavor sector is made, i.e., $|V_{eN}|$ is kept nonzero and set $|V_{\mu N}|, |V_{\tau N}| = 0$. Only one heavy neutrino



mass eigenstate is considered. SM inputs are fixed according to the values in Ref. [228].

3.1.2 Axion-like particles

To study the production ALPs a from Z decays at FCC-ee, the process

$$\text{ALP: } e^+e^- \rightarrow Z \rightarrow a\gamma, \quad \text{with } a \rightarrow \gamma\gamma, \quad (23)$$

is simulated using the model libraries of Ref. [188] in conjunction with MadGraph5_aMC@NLO. These libraries implement the Lagrangian described in Section 2.2.

3.1.3 Exotic Higgs boson decays

A simulation study of exotic Higgs decays into LLPs is left for a future paper, as well as additional detector concepts, namely the CLIC-like detector (CLD) design [232].

3.2 Heavy neutral leptons

Although the most promising Seesaw models feature two or three HNL states in the same mass range, and possibly almost degenerate, a reasonable experimental approach is to begin by considering the production and decay of a single HNL particle.

The branching fraction of a Z boson decay into any light neutrino or antineutrino and a heavy neutrino N , which mixes with the three families of neutrinos is given by [97, 233]:

TABLE 1 The cross section and expected number of events at 150 ab^{-1} , for an HNL with a mass of 50 GeV and for several choices of $|V_{eN}|$.

Active-sterile mixing $ V_{eN} $	Cross Section [pb]	Expected events at 150 ab^{-1}
1×10^{-1}	2.29	343,200,000
1×10^{-2}	2.29×10^{-2}	3,432,000
1×10^{-3}	2.29×10^{-4}	34,320
1×10^{-4}	2.29×10^{-6}	343
1×10^{-5}	2.29×10^{-8}	3
1×10^{-6}	2.29×10^{-10}	0

No event selection is applied.

$$\text{BR}(Z \rightarrow \nu N) = \frac{2}{3}|U_N|^2 \text{BR}(Z \rightarrow \text{invisible}) \left(1 + \frac{m_N^2}{2m_Z^2}\right) \times \left(1 - \frac{m_N^2}{m_Z^2}\right), \quad (24)$$

where $|U_N|^2 \equiv \sum_{\ell=e,\mu,\tau} |U_{\ell N}|^2$ is the sum of the mixing matrix elements of the HNL N with the three active neutrinos ν_ℓ . As the HNL masses considered here are much heavier than the tau lepton, the total charged current decay rate of the HNL $N \rightarrow \ell_\lambda W^*$ is also proportional to the same combination of mixing angles.

$$\Gamma_N = \frac{1}{c\tau_N} \approx C_0 C_{MD} |U_N|^2 \left(\frac{m_N}{50\text{GeV}}\right)^5 \times \left(\frac{3 \cdot 10^9}{1 \text{ cm}}\right) \quad (25)$$

Here, C_0 is a numerical coefficient of $\mathcal{O}(1)$ that takes into account the open charged- and neutral-current decays of the heavy neutrino, and C_{MD} is a coefficient that depends on the Dirac ($C_{MD} = 1$) or Majorana ($C_{MD} = 2$) nature of the particle, since twice as many decay channels are open for the Majorana particle decay. Potentially, with sufficient statistics, the direct comparison of the event rate with the lifetime for an HNL of a known mass would allow a discrimination between a Dirac and a Majorana particle.

The corresponding decay length is then of the order of a meter for a 50 GeV HNL. In those conditions, a HNL would decay in the volume of an FCC-ee detector, leading to the observable signature of a displaced vertex, with a significant time delay (several nanoseconds) with respect to ultra relativistic particles. This leads to a particularly clean signature, for which a first analysis [39] argued that it could be a background-free search, at least for the dominant charged current decay $N \rightarrow \ell W^* \rightarrow \ell + \text{hadrons}$. Figure 10 shows what such a possible decay of the N at a future FCC-ee experiment would look like, in this case for a semileptonic final state.

Furthermore, for $Z \rightarrow N\nu_\ell$ decays, the two-body Z decay kinematics results in a mono-chromatic HNL.

Therefore, even in cases where a full, final-state reconstruction is not possible, a simultaneous measurement of

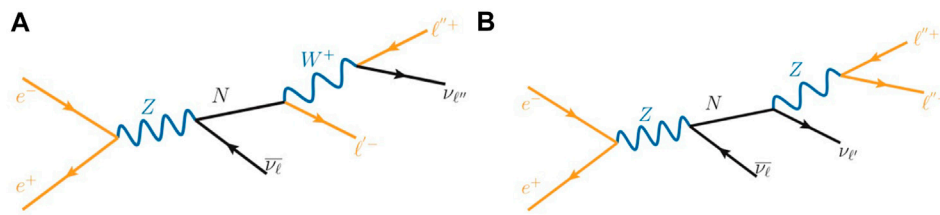


FIGURE 11
Representative diagrams depicting the $e^+e^- \rightarrow Z \rightarrow N\nu_\ell$ process at leading order, with N decaying via (A) charged current and (B) neutral current channels to the two-neutrino, two-charged lepton final state.

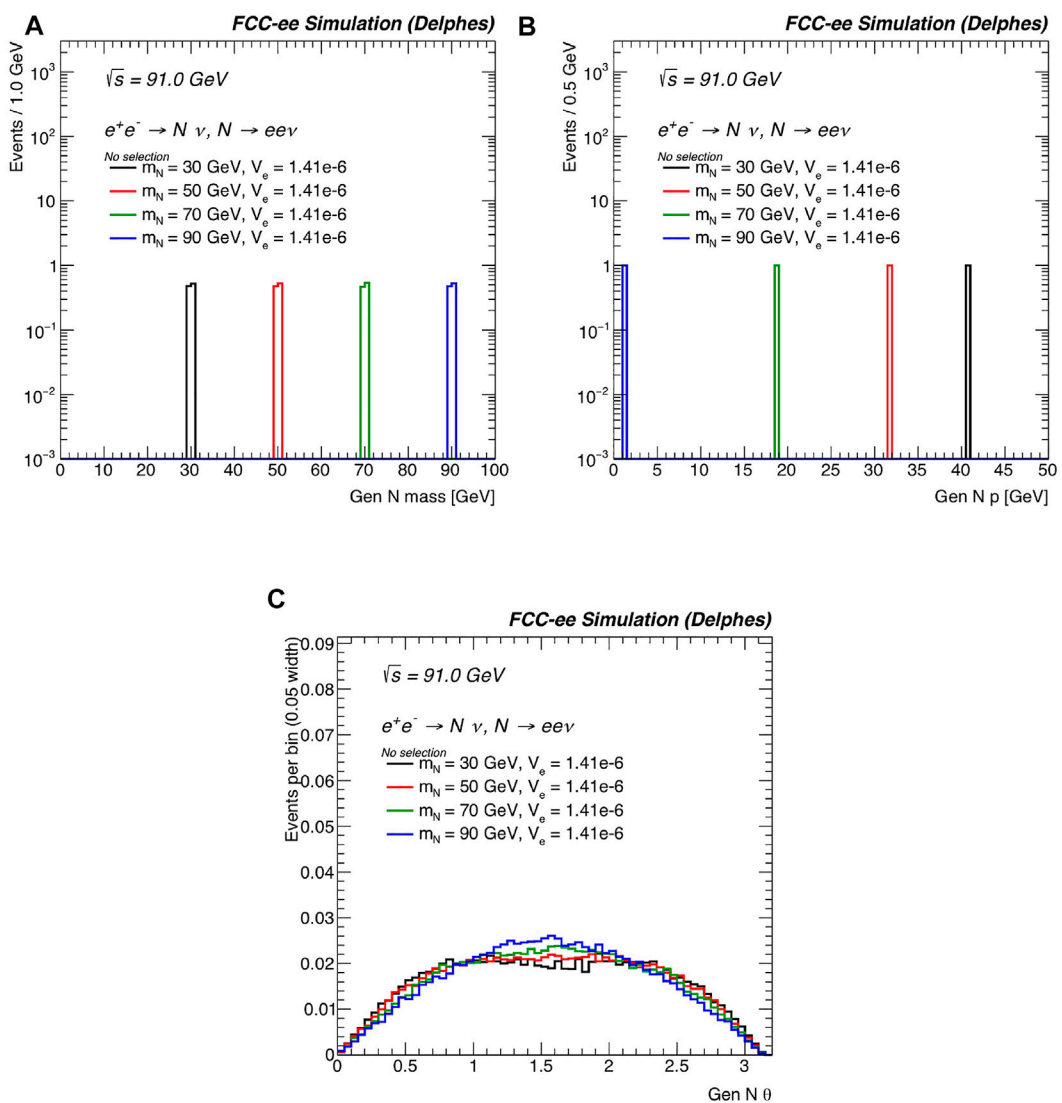


FIGURE 12
For the processes $e^+e^- \rightarrow N\nu_\ell + N\bar{\nu}_\ell$ with $N \rightarrow e^+e^-\nu_\ell + e^+e^-\bar{\nu}_\ell$ at $\sqrt{s} = 91$ GeV, the generator-level distributions of (A) the invariant mass of N , (B) the magnitude of N 's three-momentum in the lab frame, and (C) the polar angle of N with respect to the beam axis in the lab frame are shown, for representative HNL masses and representative active-sterile mixing $|V_{eN}| = 1.41 \times 10^{-6}$. The distributions are normalized to unit area.

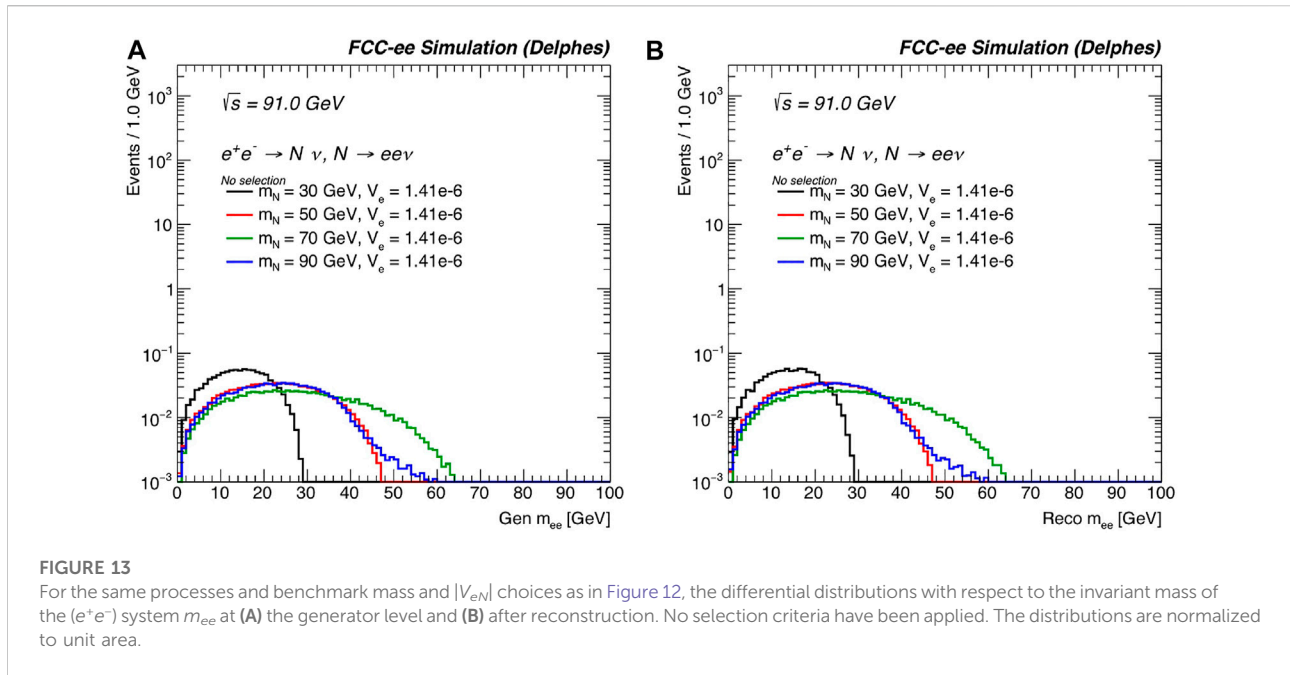


FIGURE 13

For the same processes and benchmark mass and $|V_{eN}|$ choices as in Figure 12, the differential distributions with respect to the invariant mass of the (e^+e^-) system m_{ee} at (A) the generator level and (B) after reconstruction. No selection criteria have been applied. The distributions are normalized to unit area.

the decay path and of the time-of-flight provides a determination of both the mass and proper decay time on an event-by-event basis. A detailed simulation of the process is thus of great interest to understanding how much statistics are required, first to establish the existence of the new particle, and then to establish the possible existence of a lepton number violating process (Majorana vs. Dirac nature). This also leads to the identification of specific detector requirements to optimize the discovery potential.

3.2.1 Production and kinematics of electroweak-scale HNLs

As a first step to exploring the sensitivity of FCC-ee to EW-scale HNLs, Table 1 shows the cross section (center column) and the expected number of events (right column) for an HNL with a mass of $m_N = 50$ GeV when produced and decayed through the process described in Eq. 22 and shown in Figure 11.

Results are shown for several choices of active-sterile mixing $|V_{eN}|$, and assume that an integrated luminosity of 150 ab^{-1} is collected during the Tera-Z run of FCC-ee [3]. No event selection is applied at this stage.

The kinematics of HNLs in the $m_N = 20\text{--}90$ GeV mass range at FCC-ee can also be studied. Figure 12 shows the baseline kinematics distributions of N when no event selection is applied at this stage. Here and below, active-sterile mixing of $|V_{eN}| = 1.41 \times 10^{-6}$ for representative masses of $m_N = 30$ (50) [70] {90} GeV is assumed.

Figure 12A shows the generator-level invariant mass of the HNL, which aligns with the pole mass of N . In Figure 12B, the

magnitude of the normalized, generator-level three-momentum $|\vec{p}_N|$ in the lab frame is presented. From elementary kinematics, $|\vec{p}_N|$ is given analytically for a massless electron by the formula

$$|\vec{p}_N| = \frac{M_Z}{2} \left(1 - \frac{m_N^2}{M_Z^2} \right). \quad (26)$$

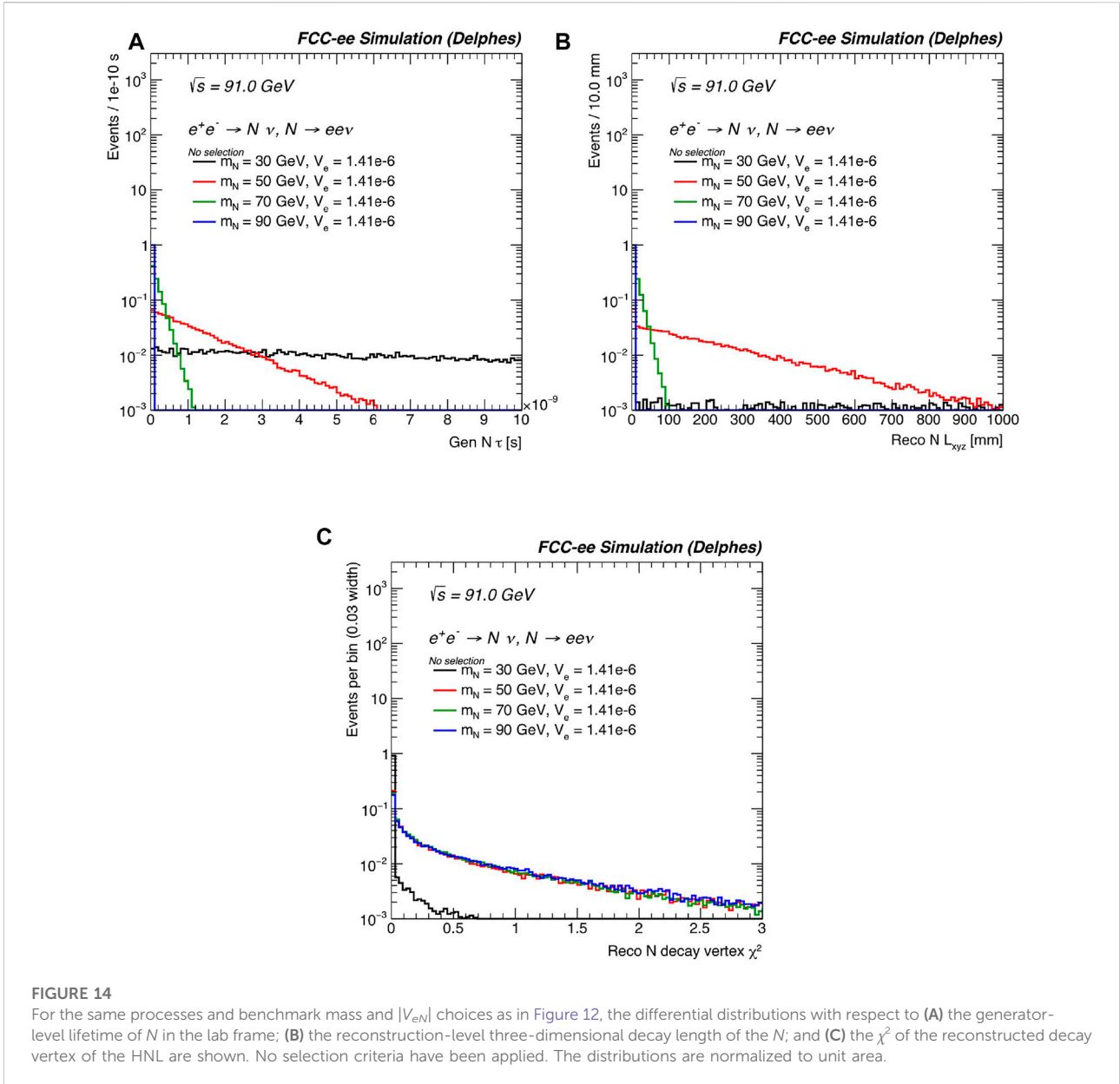
This corresponds to $|\vec{p}_N| \approx 40.7$ (31.9) [18.7] {1.2} GeV for the representative m_N under consideration and is in good agreement with the values $|\vec{p}_N| \approx 41$ (32) [19] {1.2} GeV shown in Figure 12B. Finally, the generator-level polar angle θ of N with respect to the beam axis in the lab frame is presented in Figure 12C. The distribution shows that a bulk of events feature central ($0.5 < \theta < 2.5$) HNLs, as one would expect from a high- p_T process.

To explore the potential impact of finite detector resolution, limited geometric coverage, and detector mismeasurements, Figure 13 shows the distributions with respect to the invariant mass of the (e^+e^-) system, which is given for massless electrons by the formula

$$m_{ee} = \sqrt{(p_{e^+} + p_{e^-})^2} \approx \sqrt{2p_{e^+} \cdot p_{e^-}} = \sqrt{2E_{e^+}E_{e^-}(1 - \cos\theta_{ee})}, \quad (27)$$

at (a) the generator level (Gen) and (b) the reconstruction level (Reco). In both cases, no selection criteria have been applied and the same representative inputs as above are assumed.

Consider first the generator-level case in Figure 13A. As both charged leptons in the final state originate from the $N \rightarrow$



e^+e^-X decay, the distribution of m_{ee} is dictated by the properties of N itself. For instance: for each of the mass benchmarks, the value of the observable m_{ee} does not exceed m_N itself, i.e., $\max(m_{ee}) < m_N$. This can be understood from momentum conservation:

$$m_N^2 = (p_{e^+} + p_{e^-} + p_\nu)^2 = p_\nu^2 + 2(p_\nu \cdot p_{e^+}) + 2(p_\nu \cdot p_{e^-}) + m_{ee}^2 \geq m_{ee}^2. \quad (28)$$

When m_{ee} is close to m_N , one can infer that the final-state neutrino carries little-to-no energy. For $m_N = 90$ GeV, kinematic peculiarities arise due to threshold effects. More

specifically, since $\sqrt{s} = 91$ GeV, one can consider N to be essentially at rest when $m_N = 90$ GeV. For such masses, the two-body decay $N \rightarrow e^\pm W^\mp$ becomes kinematically favored. The energy of this first electron and W are given approximately by formulae similar to Eq. 26, and come out to be $E_1 \approx 9.4$ GeV and $E_W \approx 80.6$ GeV.

Assuming that the decay products of the W boson are configured in the lab frame such that the second electron carries away all the energy of W , i.e., $E_2 \approx E_W$, then the formula for m_{ee} shows that the maximum invariant mass for $m_N = 90$ GeV is about $\max(m_{ee}) \approx \sqrt{4(9.4 \text{ GeV})(80.6 \text{ GeV})} \approx 55$ GeV. This is in agreement with Figure 13A.

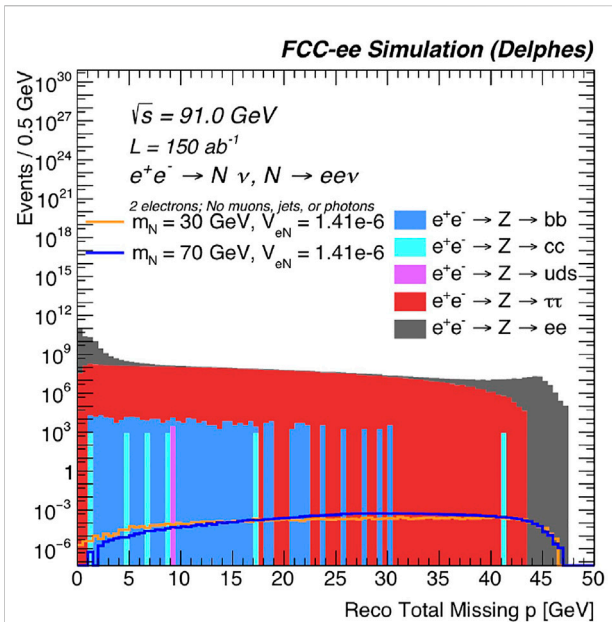


FIGURE 15
The normalized, reconstructed-level total missing momentum, for representative HNL signal benchmark mass and $|V_{eN}|$ choices, as well as background processes. Exactly two reconstructed electrons are required, as well as that there are no reconstructed muons, jets or photons in each event.

Comparing Figures 13A,B demonstrates some impact of the event reconstruction. Importantly, many of the kinematic features found at the generator level survive at the

reconstruction level. In particular, the endpoints of m_{ee} are preserved. Likewise, the means of each distribution, which span about $m_{ee}^{mean} \approx 14 - 28$ GeV, remain unaltered at the reconstruction level. The relatively small impact of reconstruction effects can be tied to the high requirements of the FCC sub-detector systems.

In the absence of additional new physics, HNLs with masses below the EW scale and active-sterile mixing much smaller than unity are generically long-lived. To explore this at FCC-ee, Figure 14 shows (a) the generator-level lifetime (s) of N , given by $\tau = \gamma_N \tau_N$, where $\gamma_N = E_N/m_N$ is the Lorentz boost of N in the lab frame, and τ_N is the proper lifetime; (b) the reconstructed three-dimensional decay length (mm) of the HNL (L_{xyz}); and (c) the χ^2 of the reconstructed displaced vertex.

For a fixed width of $|V_{eN}| = 1.41 \times 10^{-6}$, different qualitative features can be observed for the representative m_N . For instance, at $m_N = 30$ GeV, characteristic generator-level lifetimes readily exceed several seconds. This implies displaced vertices can be well beyond one or more meters, and therefore outside the fiducial coverage of the IDEA detector. In these instances, a large region of the event's phase space corresponds to long-lived HNLs that ostensibly appear as missing momentum.

For heavier N , lifetimes are drastically smaller, with most HNL events exhibiting a lifetime of less than 1–2 s for $m_N \geq 50$ GeV. For $m_N = 50$ (70) GeV, such lifetimes correspond to reconstructed displacements that are mostly within $L_{xyz} = 50$ (100) mm. Finally, in Figure 14C, the χ^2 curves indicate that the displaced vertices are well-reconstructed, with small χ^2 values.

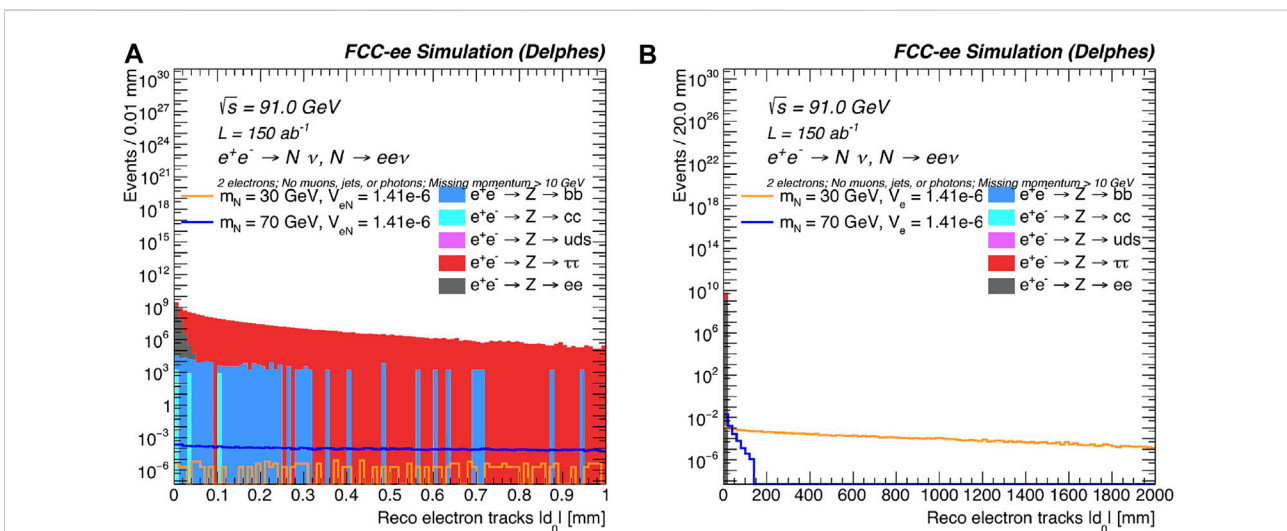


FIGURE 16
The normalized, reconstructed-level absolute value of the transverse impact parameter $|d_0|$, for representative HNL signal benchmark mass and $|V_{eN}|$ choices, as well as background processes, for (A) 0–1 mm in $|d_0|$ and (B) 0–2000 mm in $|d_0|$. Exactly two reconstructed electrons are required, as well as that there are no reconstructed muons, jets or photons in each event. The total missing momentum must be greater than 10 GeV.

TABLE 2 The expected number of events at an integrated luminosity of 150 ab^{-1} is shown for the background processes, for each selection criterion.

	Before selection	Exactly 2 reco e	Vetoos	$p/ > 10 \text{ GeV}$	$ d_0 > 0.5 \text{ mm}$
$Z \rightarrow ee$	$2.19 \times 10^{11} \pm 6.94 \times 10^7$	$1.75 \times 10^{11} \pm 6.19 \times 10^7$	$1.53 \times 10^{11} \pm 5.80 \times 10^7$	$7.07 \times 10^8 \pm 3.94 \times 10^6$	$\leq 3.94 \times 10^6$
$Z \rightarrow bb$	$9.97 \times 10^{11} \pm 4.14 \times 10^7$	$5.64 \times 10^8 \pm 9.85 \times 10^5$	$3.25 \times 10^5 \pm 2.36 \times 10^4$	$1.22 \times 10^5 \pm 1.45 \times 10^4$	$1.72 \times 10^3 \pm 1.72 \times 10^3$
$Z \rightarrow \tau\tau$	$2.21 \times 10^{11} \pm 7.00 \times 10^7$	$5.49 \times 10^9 \pm 1.10 \times 10^7$	$5.10 \times 10^9 \pm 1.06 \times 10^7$	$2.52 \times 10^9 \pm 7.47 \times 10^6$	$6.64 \times 10^4 \pm 3.84 \times 10^4$
$Z \rightarrow cc$	$7.82 \times 10^{11} \pm 2.61 \times 10^7$	$1.69 \times 10^7 \pm 1.21 \times 10^5$	$5.22 \times 10^3 \pm 2.13 \times 10^3$	$1.74 \times 10^3 \pm 1.23 \times 10^3$	$\leq 1.23 \times 10^3$
$Z \rightarrow uds$	$2.79 \times 10^{12} \pm 8.83 \times 10^7$	$2.30 \times 10^7 \pm 2.54 \times 10^5$	$2.79 \times 10^3 \pm 2.79 \times 10^3$	$\leq 2.79 \times 10^3$	$\leq 2.79 \times 10^3$

The cumulative number of events is shown. Only statistical uncertainty is taken into account.

TABLE 3 The expected number of events at an integrated luminosity of 150 ab^{-1} is shown for representative HNL signal benchmark masses and $|V_{eN}|$ choices, for each selection criterion.

	Before selection	Exactly 2 reco e	Vetoos	$p/ > 10 \text{ GeV}$	$ d_0 > 0.5 \text{ mm}$
$m_N = 10 \text{ GeV}, V_{eN} = 2 \times 10^{-4}$	2534 ± 11	1006 ± 7	996 ± 7	951 ± 7	907 ± 7
$m_N = 20 \text{ GeV}, V_{eN} = 9 \times 10^{-5}$	458 ± 2	313 ± 2	308 ± 2	293 ± 2	230 ± 1
$m_N = 20 \text{ GeV}, V_{eN} = 3 \times 10^{-5}$	51.0 ± 0.2	34.7 ± 0.2	34.2 ± 0.2	32.6 ± 0.2	31.2 ± 0.2
$m_N = 30 \text{ GeV}, V_{eN} = 1 \times 10^{-5}$	5.01 ± 0.02	3.85 ± 0.02	3.76 ± 0.02	3.54 ± 0.02	3.39 ± 0.02
$m_N = 50 \text{ GeV}, V_{eN} = 6 \times 10^{-6}$	1.23 ± 0.01	0.99 ± 0.01	0.96 ± 0.01	0.92 ± 0.01	0.729 ± 0.004

The cumulative number of events is shown. Only statistical uncertainty is taken into account.

3.2.2 Backgrounds and event selection

Several backgrounds to the HNL processes described in Eq. 22a, Eq. 22b are considered, namely, Z bosons that decay to electron-positron pairs, to tau pairs, to light quarks, to charm quark pairs, and to b quark pairs. These background processes were simulated with the conditions described above.

Figures 15, 16 show distributions of variables that distinguish the HNL signal from these background processes. Figure 15 shows the total missing momentum p_{in} each event. Unlike in a hadron collider, where only the missing momentum in the transverse direction can be considered, the three-dimensional missing momentum can be used at FCC-ee. As can be seen from this figure, requiring $p/ > 10 \text{ GeV}$ significantly reduces the background contributions while maintaining a high efficiency for the HNL signal.

Figure 16 shows the electron-track transverse impact parameter $|d_0|$ for each event. The transverse impact parameter is the distance of closest approach in the transverse plane of the helical trajectory of the track with respect to the beam axis; it is a measurement of the reconstructed electron's displacement. Requiring that both electron tracks have $|d_0| > 0.5 \text{ mm}$ removes the vast majority of the background.

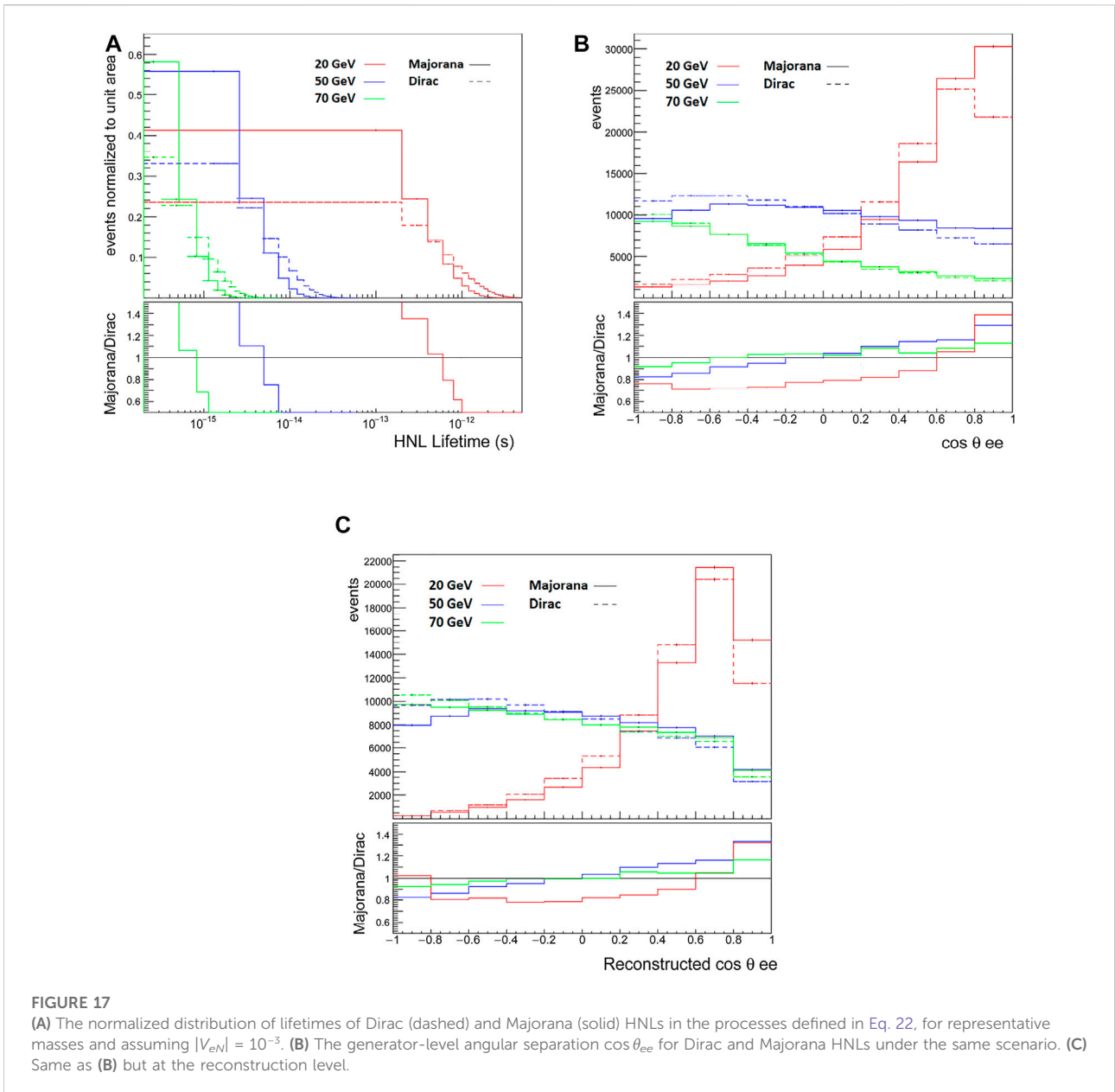
Taking these and other distributions into account, a simple event selection is developed, using reconstructed-level variables. Events must have exactly two electrons, and no photons, jets, or muons. These requirements

substantially reduce the background from light and heavy quarks. We next require $p/ > 10 \text{ GeV}$, which is particularly effective at reducing $Z \rightarrow ee$ events with spurious missing momentum associated with finite detector resolution. Finally, we require that both electrons are displaced with $|d_0| > 0.5 \text{ mm}$ to remove the vast majority of the remaining (prompt) backgrounds.

Table 2 shows the expected number of background events for each cumulative selection criterion, and Table 3 shows the same for representative HNL signal benchmark masses and $|V_{eN}|$ choices, assuming an integrated luminosity of 150 ab^{-1} . Within these limitations, these tables show that after all the selection criteria are applied, the background can be substantially reduced while the majority of the signal events are retained. After all the selection criteria are applied, we can expect about 1 event for an HNL with a mass of 50 GeV and $|V_{eN}| = 6 \times 10^{-6}$, with an integrated luminosity of 150 ab^{-1} . This benchmark point is illustrative of the maximum sensitivity to long-lived HNLs that can be achieved at FCC-ee, with the current study.

3.2.3 Majorana and Dirac nature of the HNL

If HNLs exist in nature, a chief goal is to ascertain whether they are Dirac or Majorana fermions. As discussed in Section 2.1 and elsewhere [33, 120–122], determining this is tantamount to observing processes that are mediated by N and exhibit LNV. However, at FCC-ee, the net lepton numbers of the processes $e^+e^- \rightarrow N\gamma_\ell + N\bar{\nu}_\ell$ with $N \rightarrow (\text{anything})$ are

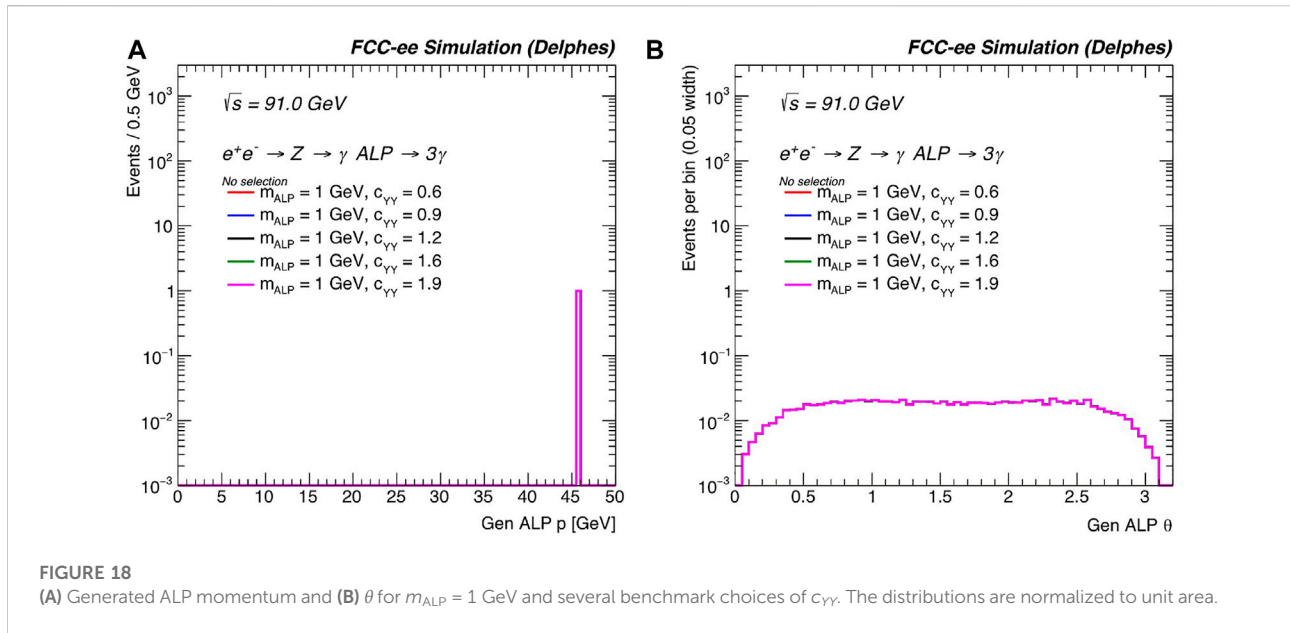


hidden because light neutrinos are not detected. This implies other metrics, such as angular distributions, are needed to disentangle the situation when lepton number violating states cannot be unambiguously identified.

To demonstrate the ability of FCC-ee to potentially disentangle the Dirac or Majorana nature of HNLs, the cleanest fully-leptonic decay channels are studied; the semileptonic decay channels have about twice as large a branching ratio and will be considered in future studies. Figure 17 shows the comparison of generator- and reconstruction-level observables for the two processes

defined in Eq. 22. An important distinction to reiterate is that the Majorana HNL channel (solid line) includes final states that are both lepton number-conserving ($e^+e^-\nu_e\bar{\nu}_e$) as well as final states that are lepton number-violating ($e^+e^-\nu_e\nu_e, e^+e^-\bar{\nu}_e\bar{\nu}_e$). On the other hand, the Dirac HNL channel (dashed line) consists only of final states that are lepton number-conserving ($e^+e^-\nu_e\bar{\nu}_e$). Therefore, kinematical differences amount to differences between LNV and LNC.

Figure 17A shows the normalized distribution of lifetimes of Dirac and Majorana HNLs for representative masses and



assuming $|V_{eN}| = 10^{-3}$. Systematically, the lifetimes for Dirac N are twice as large as for the Majorana case. For $m_N = 20\text{--}70$ GeV, the lifetimes are roughly $\tau \sim \mathcal{O}(10^{-11}) - \mathcal{O}(10^{-15})$ s. As shown in Eqs 24, 25, the lifetime measurement can be used together with the total cross section to distinguish between the Dirac or Majorana nature of the observed HNL, because the combination of mixing angles that appears in both quantities is the same. For this to be done correctly, two more conditions must be met. First, the mass of the HNL must be known; this can be done by direct reconstruction, possibly combined with a kinematic fit if the HNL decays within the good quality tracker and calorimeter volumes. For longer lifetimes, a combination of decay length and laboratory decay time should be sufficient. Second, the event selection must have similar and well understood efficiencies for the three lepton flavors e, μ, τ , so that the differences can be corrected.

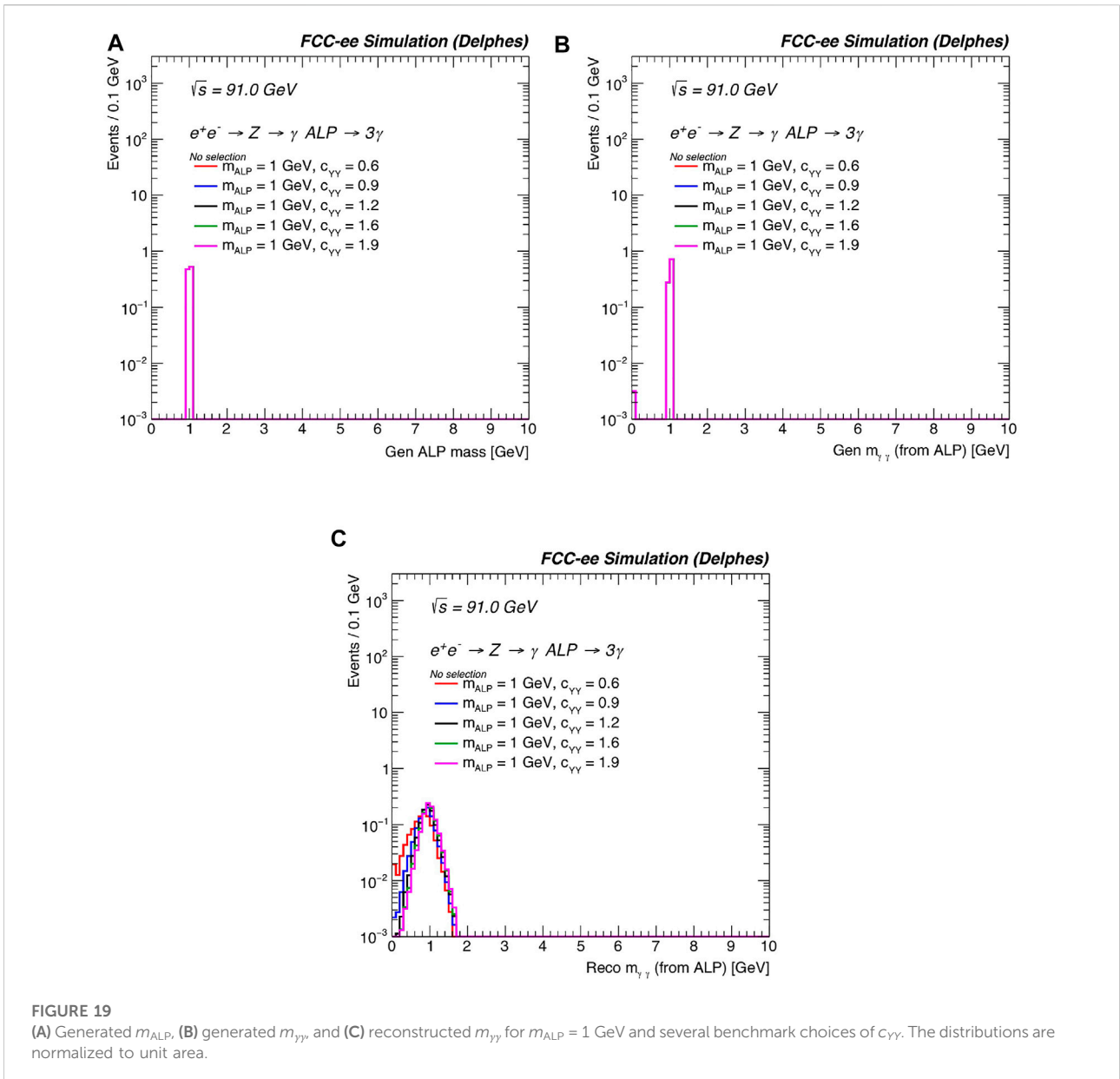
For the same scenario, Figure 17B shows the angular separation $\cos\theta_{ee}$ of the e^+e^- pair at the generator level. Here, several features can be observed. First, for small (large) m_N , the e^+e^- pair are largely collimated (back-to-back). This behavior can be understood from the kinematics: a heavier N is produced with less three-momentum, leading to three-body decays that are more isotropically distributed, whereas a lighter N is produced with more energy, which leads to more collimated decay products. The second feature that can be observed is that differences between the Majorana channel (LNC + LNV) and

the Dirac channel (LNC) can reach $\mathcal{O}(\pm 30\%)$. Differences are largest when the e^+e^- pair are collimated ($\cos\theta_{ee} \approx 1$) or back-to-back ($\cos\theta_{ee} \approx -1$), and are smallest when they are orthogonal ($\cos\theta_{ee} \approx 0$).

Finally, Figure 17C shows the same angular separation at the reconstruction level. Again, several features can be observed. First is that reconstruction requirements markedly impact the $\cos\theta_{ee}$. In particular, isolation requirements significantly reduce cases where the e^+e^- pair are collimated ($\cos\theta_{ee} \approx 1$). Overall, the distribution for $m_N = 50$ GeV and $m_N = 70$ GeV become essentially indistinguishable. Moreover, differences between the Majorana channel (LNC + LNV) and the Dirac channel (LNC) can reduce to the $\mathcal{O}(\pm 20\%)$ level.

3.3 Axion-like particles

Figure 18 shows the generated ALP kinematics for $m_{\text{ALP}} = 1$ GeV and several benchmark choices of the hypercharge coupling $c_{\gamma\gamma}$. Figure 19 shows the generated ALP mass (m_{ALP}) and the invariant mass of the two-photon system ($m_{\gamma\gamma}$), and Figure 20 shows the generated three-dimensional lifetime τ_{xyz} and decay length L_{xyz} for the ALP signal. These variables are useful in distinguishing the ALP signal from background, and also for different values of the ALP mass and couplings. In addition, calorimeter and precision timing variables will be extremely helpful to include in this study



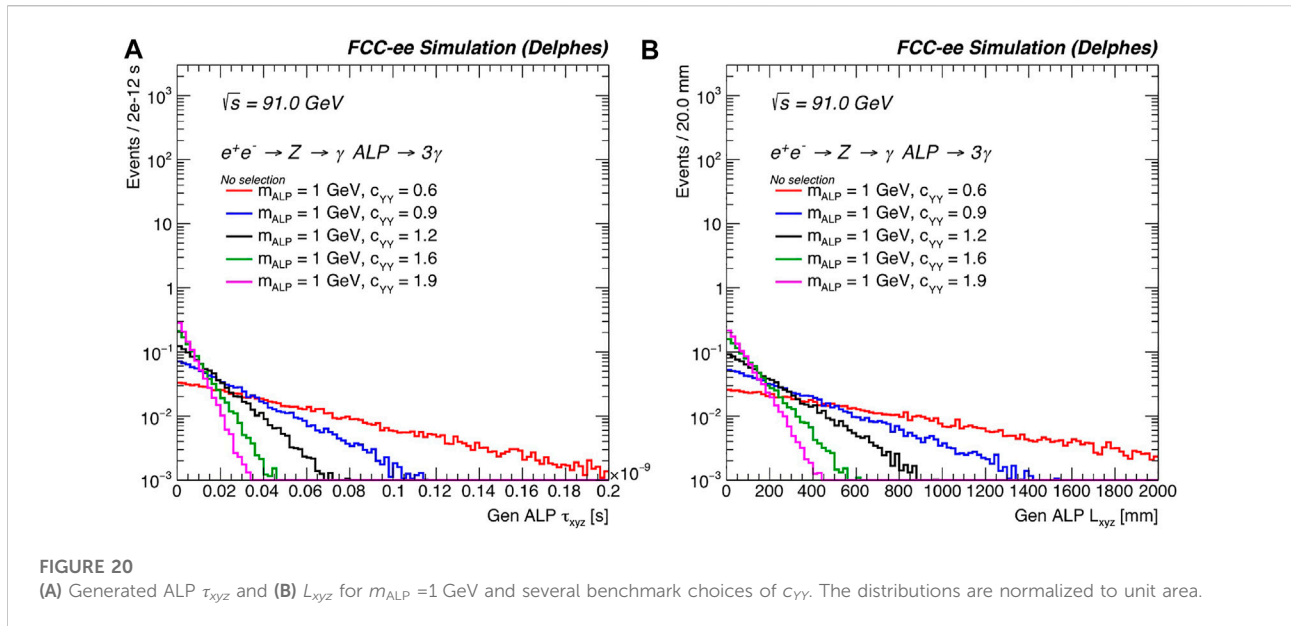
of ALPs that decay to photons. We leave these studies to a later date.

3.4 Exotic Higgs boson decays

Exotic decays of Higgs bosons to LLPs are also an interesting experimental case study at FCC-ee. As was pointed out in Section 2.3, hadronic final states play a significant role, and so we plan to simulate this physics benchmark in a future paper.

3.5 Additional detectors for long-lived particles

It is possible to envisage up to four FCC-ee detectors, two of which sitting in the very large caverns foreseen from the start for the subsequent hadron collider detectors. The caverns are foreseen to be deep (200–300 m) underground, considerably reducing the cosmic ray backgrounds. A detector fully optimized for this important discovery possibility can thus be considered [83, 110, 194].



4 Summary and conclusion

In this paper, we discuss three key BSM cases at the future FCC-ee that experimentally can display long-lived signatures: heavy neutral leptons, axion-like particles, and exotic Higgs boson decays. While FCC-ee is primarily envisioned as a precision collider, the discussed scenarios are examples of direct searches that could be performed and could answer central questions of particle physics.

The three cases are carefully discussed from a theoretical perspective, representing the state-of-the-art and current best expected limits. Simulation studies are then presented for HNLs and ALPs. These two BSM cases can present displaced signatures: a displaced vertex for the former, and a displaced photon pair in the latter.

Different HNL signals—as well as a limited collection of background processes—are generated, kinematic variables are explored, and a first possible set of requirements is presented to isolate the signal from the SM backgrounds. Possible kinematic variables that could characterize an HNL as Dirac or Majorana are also explored experimentally.

For ALPs, signals are generated and validated and some key distributions are presented.

The work presented here can be expanded into more detailed studies, such as also including exotic Higgs boson decays, additional HNL decay channels, larger simulated samples, the use of timing information, and alternative detector designs. The simulation work presented here

represents the first step towards a comprehensive evaluation of the experimental potential of FCC-ee in direct searches for BSM. Possible limitations could be solved by innovative experimental solutions that could boost the reach of FCC-ee for other non-standard signals.

Data availability statement

The raw data supporting the conclusion of this article will be made available by the authors, without undue reservation.

Author contributions

Some of the contributions are stated in the paper itself. Others involve collaboration and cross-checks. Work produced for the master theses of LR and TS is included in the paper.

Funding

RS is supported by the Swedish Research Council (VR 2017-05092). SK is supported by the Austrian Science Fund Elise-Richter grant project number V592-N27. RR acknowledges the support of the Polska Akademia Nauk (grant agreement PAN.BFD.S.BDN. 613. 022.

2021—PASIFIC 1, POPSICLE). This work has received funding from the European Union's Horizon 2020 research and innovation program under the Skłodowska-Curie grant agreement No. 847639 and from the Polish Ministry of Education and Science. AT was supported by the Australian Research Council through the ARC Discovery Project, DP210101900.

Acknowledgments

The authors would like to thank S. Petcov (SISSA/INFN) for the discussions during the writing of the paper and for providing comments to the draft.

References

- Alimena J, Beacham J, Borsato M, Cheng Y, Vidal X. C., Cottin G et al. Searching for long-lived particles beyond the standard model at the Large Hadron Collider. *J Phys G* (2020) 47:090501. 1903.04497.
- Group ES. Update of the European Strategy for particle physics (brochure). *Tech Rep Cern-esu-015* (2020). CERN, Geneva. doi:10.17181/CERN.JSC6.W89E
- Benedikt M, Blondel A, Brunner O, Capeans Garrido M, Cerutti F, Gutleber J et al. FCC-ee: The lepton collider: Future circular collider conceptual design report volume 2. Future Circular Collider, Tech. Rep. CERN-ACC-2018-0057. 2, CERN, Geneva, 2018. doi:10.1140/epjst/e2019-900045-4
- Chrzyszcz M, Gonzalez Suarez R, Monteil S. Hunt for rare processes and long-lived particles at FCC-ee. *Eur Phys J Plus* (2021) 136(1056). [2106.15459]. doi:10.1140/epjp/s13360-021-01961-4
- Abdullahi AM, Alzas PB, Batell B, Boyarsky A, Carbajal S, Chatterjee A et al. The present and future status of heavy neutral leptons. *Snowmass Summer Study* (2022) 3:08039. 2203.
- Super-Kamiokande collaboration, Fukuda Y, Havakawa T, Ichihara I, Inoue K, Ishihara K, Ishino H et al. Evidence for oscillation of atmospheric neutrinos. *Phys Rev Lett* (1998) 81:1562–7. [hep-ex/9807003].
- SNO collaboration, Ahmad QR, Allen RC, Andersen TC, D Anglin J, Barton JC, Beier EW et al. Direct evidence for neutrino flavor transformation from neutral current interactions in the Sudbury Neutrino Observatory. *Phys Rev Lett* (2002) 89:011301. [nucl-ex/0204008]. doi:10.1103/PhysRevLett.89.011301
- Feruglio F. Pieces of the flavour puzzle. *Eur Phys J C* (2015) 75373. [1503.04071]. doi:10.1140/epjc/s10052-015-3576-5
- Ma E. Pathways to naturally small neutrino masses. *Phys Rev Lett* (1998) 81:1171–4. [hep-ph/9805219]. doi:10.1103/physrevlett.81.1171
- Agrawal P, Bauer M, Beacham J, Berlin A, Boyarsky A, Cebrian S et al. Feebly-interacting particles: FIPs 2020 workshop report. *Eur Phys J C* (2021) 81:1015. [2102.12143]. doi:10.1140/epjc/s10052-021-09703-7
- Minkowski P. $\mu \rightarrow e\gamma$ at a Rate of one Out of 10^9 muon decays? *Phys Lett B* (1977) 67:421–8. doi:10.1016/0370-2693(77)90435-x
- Glashow SL. The future of elementary particle physics. *NATO Sci Ser B* (1980) 61:687.
- Gell-Mann M, Ramond P, Slansky R. Complex spinors and unified theories. *Conf Proc C* (1979) 790927:315–21. [1306.4669].
- Mohapatra RN, Senjanovic G. Neutrino mass and spontaneous parity nonconservation. *Phys Rev Lett* (1980) 44:912–5. doi:10.1103/physrevlett.44.912
- Yanagida T. Horizontal symmetry and masses of neutrinos. *Prog Theor Phys* (1980) 64:1103–5. doi:10.1143/ptp.64.1103
- Schechter J, Valle JWF. Neutrino masses in $SU(2) \otimes U(1)$ theories. *Phys Rev D* (1980) 22:2227–35. doi:10.1103/physrevd.22.2227
- Shrock RE. General theory of weak processes involving neutrinos. I. Leptonic pseudoscalar-meson decays, with associated tests for, and bounds on, neutrino masses and lepton mixing. *Phys Rev D* (1981) 24:1232–74. doi:10.1103/physrevd.24.1232
- Konetschny W, Kummer W. Nonconservation of total lepton number with scalar bosons. *Phys Lett B* (1977) 70:433–5. doi:10.1016/0370-2693(77)90407-5

Conflict of interest

The authors declare that the research was conducted in the absence of any commercial or financial relationships that could be construed as a potential conflict of interest.

Publisher's note

All claims expressed in this article are solely those of the authors and do not necessarily represent those of their affiliated organizations, or those of the publisher, the editors and the reviewers. Any product that may be evaluated in this article, or claim that may be made by its manufacturer, is not guaranteed or endorsed by the publisher.

- Magg M, Wetterich C. Neutrino mass problem and gauge hierarchy. *Phys Lett B* (1980) 94:61–4. doi:10.1016/0370-2693(80)90825-4
- Cheng TP, Li L-F. Neutrino masses, mixings, and oscillations in $SU(2) \times U(1)$ models of electroweak interactions. *Phys Rev D* (1980) 22:2860–8. doi:10.1103/physrevd.22.2860
- Lazarides G, Shafi Q, Wetterich C. Proton lifetime and fermion masses in an $SO(10)$ model. *Nucl Phys B* (1981) 181:287–300. doi:10.1016/0550-3213(81)90354-0
- Mohapatra RN, Senjanovic G. Neutrino masses and mixings in gauge models with spontaneous parity violation. *Phys Rev D* (1981) 23:165–80. doi:10.1103/physrevd.23.165
- Foot R, Lew H, He XG, Joshi GC. Seesaw neutrino masses induced by a triplet of leptons. *Z Phys C - Particles Fields* (1989) 44:441–4. doi:10.1007/bf01415558
- Atre A, Han T, Pascoli S, Zhang B. The search for heavy Majorana neutrinos. *JHEP* (2009) 05030. 0901.3589.
- Deppisch FF, Bhupal Dev PS, Pilaftsis A. Neutrinos and collider physics. *New J Phys* (2015) 17:075019. [1502.06541]. doi:10.1088/1367-2630/17/7/075019
- Cai Y, Han T, Li T, Ruiz R. Lepton number violation: Seesaw models and their collider tests. *Front Phys* (2018) 6:40. [1711.02180]. doi:10.3389/fphy.2018.00040
- Bolton PD, Deppisch FF, Bhupal Dev PS. Neutrinoless double beta decay versus other probes of heavy sterile neutrinos. *JHEP* (2020) 03170. 1912.03058.
- Wolfenstein L. Different varieties of massive Dirac neutrinos. *Nucl Phys B* (1981) B186:147–52. doi:10.1016/0550-3213(81)90096-1
- Petcov ST. On pseudo-Dirac neutrinos, neutrino Oscillations and neutrinoless double β -decay. *Phys Lett B* (1982) 110B:245–9. doi:10.1016/0370-2693(82)91246-1
- Shaposhnikov M. A possible symmetry of the. *Nucl Phys B* (2007) 763:49–59. [hep-ph/0605047]. doi:10.1016/j.nuclphysb.2006.11.003
- Kersten J, Smirnov AY. Right-handed neutrinos at CERN LHC and the mechanism of neutrino mass generation. *Phys Rev D* (2007) 76:073005. [0705.3221]. doi:10.1103/physrevd.76.073005
- Ibarra A, Molinaro E, Petcov ST. *TeV scale see-saw Mechanisms of neutrino mass generation, the Majorana Nature of the heavy singlet Neutrinos and $(\beta\beta)_{0\nu}$ -Decay*. *JHEP* (2010) 09108. [1007.2378].
- Moffat K, Pascoli S, Weiland C. (2017) Equivalence between massless neutrinos and lepton number conservation in fermionic singlet extensions of the Standard Model, 1712.07611.
- Anamiati G, Hirsch M, Nardi E. Quasi-Dirac neutrinos at the LHC. *JHEP* (2016) 10010. [1607.05641].
- Tsai Y-S. *Decay Correlations of Heavy Leptons in $e^+e^- \rightarrow Lepton^+ Lepton^-$* . *Phys Rev D* (1971) 4:2821.
- Gronau M, Leung CN, Rosner JL. Extending limits on neutral heavy leptons. *Phys Rev D* (1984) 29:2539–58. doi:10.1103/physrevd.29.2539

37. Petcov ST. Possible signature for production of Majorana particles in e^+e^- and p - p collisions. *Phys Lett B* (1984) B 139:421–6. doi:10.1016/0370-2693(84)91844-6
38. Dittmar M, Santamaria A, Gonzalez-Garcia MC, Valle JWF. *Production Mechanisms and Signatures of isosinglet neutral heavy Leptons in Z^0 decays*. *Nucl Phys B* (1990) 332:1–19. doi:10.1016/0550-3213(90)90028-c
39. FCC-ee study Team collaboration, Blondel A, Graverini E, Serra N, Shaposhnikov M. Search for heavy right handed neutrinos at the FCC-ee. *Nucl Part Phys Proc* (2016) 1883–90. [1411.5230]. doi:10.1016/j.nuclphysbps.2015.09.304
40. Duarte L, Peressutti J, Sampayo OA. Majorana neutrino decay in an effective approach. *Phys Rev D* (2015) 92:093002. [1508.01588]. doi:10.1103/physrevd.92.093002
41. Banerjee S, Dev PSB, Ibarra A, Mandal T, Mitra M. Prospects of heavy neutrino searches at future lepton colliders. *Phys Rev D* (2015) 92:075002. doi:10.1103/physrevd.92.075002
42. Duarte L, Romero I, Peressutti J, Sampayo OA. Effective Majorana neutrino decay. *Eur Phys J C* (2016) 76453. [1603.08052]. doi:10.1140/epjc/s10052-016-4301-8
43. Antusch S, Cazzato E, Fischer O. Displaced vertex searches for sterile neutrinos at future lepton colliders. *JHEP* (2016) 12:007. [1604.02420].
44. Antusch S, Cazzato E, Drewes M, Fischer O, Garbrecht B, Gueter D et al. Probing leptogenesis at future colliders. *JHEP* (2018) 09:124. [1710.03744].
45. Duarte L, Zapata G, Sampayo OA. *Final taus and initial state polarization signatures from effective interactions of Majorana neutrinos at future e^+e^- colliders*. *Eur Phys J C* (2019) 79240. [1812.01154].
46. Ding J-N, Qin Q, Yu F-S. *Heavy neutrino searches at future Z-factories*. *Eur Phys J C* (2019) 79:766. 1903.766. doi:10.1140/epjc/s10052-019-7277-3
47. Barducci D, Bertuzzo E, Caputo A, Hernandez P, Mele B. The see-saw portal at future Higgs Factories. *JHEP* (2021) 03:117. 2011.04725.
48. Blondel A, de Gouvêa A, Kayser B. Z-boson decays into Majorana or Dirac heavy neutrinos. *Phys Rev D* (2021) 104:055027. [2105.06576]. doi:10.1103/physrevd.104.055027
49. Zapata G, Urruzola T, Sampayo OA, Duarte L. Lepton collider probes for Majorana neutrino effective interactions. *Eur Phys J C* (2022) 82(544). [2201.02480]. doi:10.1140/epjc/s10052-022-10448-0
50. Shen Y-F, Ding J-N, Qin Q. Monojet search for heavy neutrinos at future Z-factories. *Eur Phys J C* (2022) 82:398. [2201.05831]. doi:10.1140/epjc/s10052-022-10301-4
51. Barducci D, Bertuzzo E. The see-saw portal at future Higgs factories: The role of dimension six operators. *JHEP* (2022) 06:077. [2201.11754].
52. Pati JC, Salam A. Lepton number as the fourth color. *Phys Rev D* (1974) 10:275–89. doi:10.1103/physrevd.10.275
53. Mohapatra RN, Pati JC. Left-right gauge symmetry and an isoconjugate model of CP violation. *Phys Rev D* (1975) 11:566–71. doi:10.1103/physrevd.11.566
54. Mohapatra RN, Pati JC. Natural left-right symmetry. *Phys Rev D* (1975) 11:2558–61. doi:10.1103/physrevd.11.2558
55. Senjanovic G, Mohapatra RN. Exact left-right symmetry and spontaneous violation of parity. *Phys Rev D* (1975) 12:1502–5. doi:10.1103/physrevd.12.1502
56. Senjanovic G. Spontaneous breakdown of parity in a class of gauge theories. *Nucl Phys B* (1979) 153:334–64. doi:10.1016/0550-3213(79)90604-7
57. Langacker P. Grand unified theories and proton decay. *Phys Rep* (1981) 72:185–385. doi:10.1016/0370-1573(81)90059-4
58. Hewett JL, Rizzo TG. Low-energy phenomenology of superstring inspired E(6) models. *Phys Rep* (1989) 183:193–381. doi:10.1016/0370-1573(89)90071-9
59. Faraggi AE, Nanopoulos DV. *A SUPERSTRING Z' AT O(1-TeV)?* *Mod Phys Lett A* (1991) 6:61–8. doi:10.1142/s0217732391002621
60. Buchmuller W, Greub C, Minkowski P. Neutrino masses, neutral vector bosons and the scale of B-L breaking. *Phys Lett B* (1991) 267:395–9. doi:10.1016/0370-2693(91)90952-m
61. Grzadkowski B, Iskrzynski M, Misiak M, Rosiek J. Dimension-Six terms in the standard model Lagrangian. *JHEP* (2010) 10:085. [1008.4884].
62. Brivio I, Trott M. The standard model as an effective field theory. *Phys Rep* (2019) 793:1–98. [1706.08945]. doi:10.1016/j.physrep.2018.11.002
63. Gauld R, Pečjak BD, Scott DJ. One-loop corrections to h to $b\bar{b}$ and h to $\tau\bar{\tau}$ decays in the standard model dimension-6 EFT: Four-fermion operators and the large- m_t limit. *J High Energy Phys* (2016) 05:080. [1512.02508]. doi:10.1007/jhep05(2016)080
64. del Aguila F, Bar-Shalom S, Soni A, Wudka J. Heavy Majorana neutrinos in the effective Lagrangian description: Application to hadron colliders. *Phys Lett B* (2009) 670:399–402. [0806.0876]. doi:10.1016/j.physletb.2008.11.031
65. Aparici A, Kim K, Santamaria A, Wudka J. Right-handed neutrino magnetic moments. *Phys Rev D* (2009) 80:013010. [0904.3244]. doi:10.1103/physrevd.80.013010
66. Elgaard-Clausen G, Trott M. On expansions in neutrino effective field theory. *JHEP* (2017) 11(088). [1703.04415].
67. Hernández P, Kekic M, López-Pavón J, Racker J, Salvado J. Testable baryogenesis in seesaw models. *JHEP* (2016) 08157. [1606.06719].
68. Drewes M, Garbrecht B, Gueter D, Klaric J. Testing the low scale seesaw and leptogenesis. *JHEP* (2017) 08:018. 1609.09069.
69. Drewes M, Hajer J, Klaric J, Lanfranchi G. NA62 sensitivity to heavy neutral leptons in the low scale seesaw model. *JHEP* (2018) 07(105). 1801.04207.
70. Chrzyszcz M, Drewes M, Gonzalo TE, Harz J, Krishnamurthy S, Weniger C. A frequentist analysis of three right-handed neutrinos with GAMBIT. *Eur Phys J C* (2020) 80(569). 1908.569. doi:10.1140/epjc/s10052-020-8073-9
71. DUNE collaboration, Abi B, Acciarri R, Acero MA, Adamov G, Adams D, Adinolfi M et al. Deep underground neutrino experiment (DUNE), far detector technical design report, volume II: DUNE physics, 2002.03005.
72. Caputo A, Hernandez P, Kekic M, López-Pavón J, Salvado J. The seesaw path to leptonic CP violation. *Eur Phys J C* (2017) 77(258). [1611.05000]. doi:10.1140/epjc/s10052-017-4823-8
73. King SF, Luhn C. Neutrino mass and mixing with discrete symmetry. *Rep Prog Phys* (2013) 76:056201. [1301.1340]. doi:10.1088/0034-4885/76/5/056201
74. Feruglio F, Romanino A. Lepton flavor symmetries. *Rev Mod Phys* (2021) 93:015007. 1912.06028. doi:10.1103/revmodphys.93.015007
75. Xing Z-z. Flavor structures of charged fermions and massive neutrinos. *Phys Rep* (2020) 854:1–147. 1909. doi:10.1016/j.physrep.2020.02.001
76. Caputo A, Hernandez P, Lopez-Pavon J, Salvado J. The seesaw portal in testable models of neutrino masses. *JHEP* (2017) 06112. 1704.08721.
77. Esteban I, Gonzalez-Garcia M, Maltoni M, Schwetz T, Zhou A, et al. The fate of hints: Updated global analysis of three-flavor neutrino oscillations. *JHEP* (2020) 09:178. 2007.14792.
78. DUNE collaboration, Abi B, Acciarri R, Acero MA, Adamov G, Adams D, Adinolfi M et al. Long-baseline neutrino oscillation physics potential of the DUNE experiment. *Eur Phys J C* (2020) 80(978). 2006.16043.
79. Antusch S, Cazzato E, Fischer O. *Sterile neutrino searches at future e^+e^- , pp , and e^+p colliders*. *Int J Mod Phys A* (2017) 32:1750078. [1612.02728]. doi:10.1142/s0217751x17500786
80. Ellis RK, Physics briefing Book: Input for the European Strategy for particle physics update 2020, 1910.11775.
81. Lou XL. Circular electron-positron collider status and progress (presented at the hku-st-ias conference on high energy physics 2022), 2022.
82. CEPC Study Group collaboration, Dong M. CEPC conceptual design report: Volume 2. *Phys Detector* (2018) 1811:10545.
83. Chrzyszcz M, Drewes M, Hajer J. Hecate: A long-lived particle detector concept for the FCC-ee or CEPC. *Eur Phys J C* (2021) 81:546. 2011.01005. doi:10.1140/epjc/s10052-021-09253-y
84. CHARM collaboration, Dorenbosch J, Allaby JV, Amaldi U, Barbiellini G, Berger C, Bergsma F et al., A search for decays of heavy neutrinos in the mass range 0.5-GeV to 2.8-GeV. *Phys Lett B* (1986) 166:473–8.
85. Abela R, Daum M, Eaton GH, Frosch R, Jost B, Kettle PR et al. Search for an admixture of heavy neutrino states in pion decay. *Phys Lett B* (1981) 105:263–6. doi:10.1016/0370-2693(81)90884-4
86. Yamazaki T. Search for heavy neutrinos in kaon decay. *Conf Proc C* (1984) 840719:262.
87. E949 collaboration, Artamonov AV. *Search for heavy neutrinos in $K^+ \rightarrow \mu^+ \nu_H$ decays*. *Phys Rev D* (2015) 91:052001. [1411.3963].
88. Bernardi G, Carugno G, Chauveau J, Dicarolo F, Dris M, Dumarchez J et al. Further limits on heavy neutrino couplings. *Phys Lett B* (1988) 203:332–4. doi:10.1016/0370-2693(88)90563-1
89. NuTeV, E815 collaboration, Vaitaitis A, Drucker RB, Formaggio J, Koutsoliotas S, Adams T, Alton A et al. Search for neutral heavy leptons in a high-energy neutrino beam. *Phys Rev Lett* (1999) 83:4943–6. [hep-ex/9908011]. doi:10.1103/physrevlett.83.4943
90. Vaitaitis AG. Search for neutral heavy leptons in a high-energy neutrino beam. PhD thesis. New York, NY: Columbia University (2000). doi:10.2172/1421441

91. CMS collaboration, Sirunyan AM. Search for heavy neutral leptons in events with three charged leptons in proton-proton collisions at $\sqrt{s} = 13$ TeV. *Phys Rev Lett* (2018) 120:221801. 1802.02965.
92. DELPHI collaboration, Abreu P. Search for neutral heavy leptons produced in Z decays. *Z. Phys. C* (1997) 74:57–71. doi:10.1007/s002880050370
93. ATLAS collaboration, Aad G. Search for heavy neutral leptons in decays of W bosons produced in 13 TeV pp collisions using prompt and displaced signatures with the ATLAS detector. *JHEP* (2019) 10:265. 1905.09787.
94. CMS collaboration, Tumasyan A. Search for long-lived heavy neutral leptons with displaced vertices in proton-proton collisions at $\sqrt{s} = 13$. TeV (2022) 2201:05578.
95. Izaguirre E, Shuve B. Multilepton and lepton jet probes of sub-weak-scale right-handed neutrinos. *Phys Rev D* (2015) 91:093010. [1504.02470]. doi:10.1103/physrevd.91.093010
96. Drewes M, Hajer J. Heavy Neutrinos in displaced vertex searches at the LHC and HL-LHC. *JHEP* (2020) 02:070. 1903.06100.
97. Pascoli S, Ruiz R, Weiland C. Heavy neutrinos with dynamic jet vetoes: Multilepton searches at $\sqrt{s} = 14, 27$, and 100 TeV. *JHEP* (2019) 06:049. 1812.08750.
98. Ballet P, Boschi T, Pascoli S. Heavy neutral leptons from low-scale seesaws at the DUNE near detector. *JHEP* (2020) 03:111. 1905.00284.
99. FASER collaboration, Ariga A, Ariga T, Boyd J, Cadoux F, Casper DW, Favre Y et al. FASER's physics reach for long-lived particles. *Phys Rev D* (2019) 99:095011. [1811.12522]. doi:10.1103/physrevd.99.095011
100. SHiP collaboration, Ahdida C, Albanese R, Alexandrov A, Anokhina A, Aoki S, Arduini G et al. Sensitivity of the SHiP experiment to heavy neutral leptons. *JHEP* (2019) 04:077. [1811.00930].
101. Gorbunov D, Krasnov I, Kudenko Y, Suvorov S. Heavy Neutral Leptons from kaon decays in the SHiP experiment. *Phys Lett B* (2020) 810:135817. 2004.07974. doi:10.1016/j.physletb.2020.135817
102. Curtin D, Drewes M, McCullough M, Meade P, Mohapatra RN, Shelton J et al. Long-lived particles at the energy frontier: The MATHUSLA physics case. *Rep Prog Phys* (2019) 82:116201. 1806.07396. doi:10.1088/1361-6633/ab28d6
103. Aielli G, Ben-Haim E, Cardarelli R, Charles MJ, Cid Vidal X, Cocco V et al. Expression of interest for the CODEX-b detector. *Eur Phys J C* (2020) 801177. [1911.00481]. doi:10.1140/epjc/s10052-020-08711-3
104. Bay Nielsen S. Prospects of sterile neutrino search with the FCC-ee. Master's thesis. Copenhagen U. (2017).
105. Antusch S, Cazzato E, Fischer O, Hammad A, Wang K. Lepton flavor violating dilepton dijet signatures from sterile neutrinos at proton colliders. *JHEP* (2018) 10067. 1805.11400.
106. Boyarsky A, Mikulenko O, Ovchinnikov M, Shchutska L. Exploring the potential of FCC-hh to search for particles from B mesons, 2022, 2204.01622.
107. Mękała K, Reuter J, Żarnecki AF. Heavy neutrinos at future linear e^+e^- colliders. *JHEP* (2022) 06:010. 2202.06703.
108. Antusch S, Fischer O, Hammad A. Lepton-trijet and displaced vertex searches for heavy neutrinos at future electron-proton colliders. *JHEP* (2020) 03110. 1908.02852.
109. Li P, Liu Z, Lyu F-F. progress. Heavy neutral leptons at muon colliders.
110. Wang ZS, Wang K. Physics with far detectors at future lepton colliders. *Phys Rev D* (2020) 101:075046. [1911.06576]. doi:10.1103/physrevd.101.075046
111. Giffin P, Gori S, Tsai Y-D, Tucker D. Heavy neutral leptons at beam dump experiments of future lepton colliders, 2022, 2206.13745.
112. Canetti L, Drewes M, Shaposhnikov M. Matter and antimatter in the universe. *New J Phys* (2012) 14:095012. [1204.4186]. doi:10.1088/1367-2630/14/9/095012
113. Akhmedov EK, Rubakov VA, Smirnov AY. Baryogenesis via neutrino oscillations. *Phys Rev Lett* (1998) 81:1359–62. [hep-ph/9803255]. doi:10.1103/physrevlett.81.1359
114. Asaka T, Shaposhnikov M. The ν MSM, dark matter and baryon asymmetry of the universe. *Phys Lett B* (2005) 620:17–26. [hep-ph/0505013]. doi:10.1016/j.physletb.2005.06.020
115. Pilaftsis A, Underwood TEJ. Resonant leptogenesis. *Nucl Phys B* (2004) 692:303–45. [hep-ph/0309342]. doi:10.1016/j.nuclphysb.2004.05.029
116. Drewes M, Georis Y, Klarić J. Mapping the viable parameter space for testable leptogenesis. *Phys Rev Lett* (2022) 128:051801. [2106.16226]. doi:10.1103/physrevlett.128.051801
117. Klarić J, Shaposhnikov M, Timiryasov I. Reconciling resonant leptogenesis and baryogenesis via neutrino oscillations. *Phys Rev D* (2021) 104:055010. [2103.16545]. doi:10.1103/physrevd.104.055010
118. Sabti N, Magalich A, Filimonova A. An extended analysis of heavy neutral leptons during big bang nucleosynthesis. *JCAP* (2020) 11(056). 2006.07387.
119. Boyarsky A, Ovchinnikov M, Ruchayskiy O, Syvolap V. Improved big bang nucleosynthesis constraints on heavy neutral leptons. *Phys Rev D* (2021) 104:023517. 2008.00749. doi:10.1103/physrevd.104.023517
120. Schechter J, Valle JWF. Neutrinoless double- β decay in $SU(2) \times U(1)$ theories. *Phys Rev D* (1982) 25:2951–4. doi:10.1103/physrevd.25.2951
121. Hirsch M, Kovalenko S, Schmidt I. Extended black box theorem for lepton number and flavor violating processes. *Phys Lett B* (2006) 642:106–10. [hep-ph/0608207]. doi:10.1016/j.physletb.2006.09.012
122. Duerr M, Lindner M, Merle A. On the quantitative impact of the schechter-valle theorem. *JHEP* (2011) 06091. [1105.0901].
123. Bray S, Lee JS, Pilaftsis A. Resonant CP violation due to heavy neutrinos at the LHC. *Nucl Phys B* (2007) 786:95–118. [hep-ph/0702294]. doi:10.1016/j.nuclphysb.2007.07.002
124. Ruiz R. Quantitative study on helicity inversion in Majorana neutrino decays at the LHC. *Phys Rev D* (2021) 103:015022. 2008.01092. doi:10.1103/physrevd.103.015022
125. de Gouvêa A, Fox PJ, Kayser BJ, Kelly KJ. Three-body decays of heavy Dirac and Majorana fermions. *Phys Rev D* (2021) 104:015038. [2104.05719]. doi:10.1103/physrevd.104.015038
126. Hernández P, Jones-Pérez J, Suarez-Navarro O. Majorana vs pseudo-Dirac neutrinos at the ILC. *Eur Phys J C* (2019) 79220. [1810.07210]. doi:10.1140/epjc/s10052-019-6728-1
127. Asaka T, Blanchet S, Shaposhnikov M. The ν MSM, dark matter and neutrino masses. *Phys Lett B* (2005) 631:151–6. [hep-ph/0503065]. doi:10.1016/j.physletb.2005.09.070
128. Drewes M. The phenomenology of right handed neutrinos. *Int J Mod Phys E* (2013) 22:1330019. [1303.6912]. doi:10.1142/s0218301313300191
129. Fukugita M, Yanagida T. Baryogenesis without grand unification. *Phys Lett B* (1986) 174:45–7. doi:10.1016/0370-2693(86)91126-3
130. Davidson S, Ibarra A. A Lower bound on the right-handed neutrino mass from leptogenesis. *Phys Lett B* (2002) 535(25–32):25–32. [hep-ph/0202239]. doi:10.1016/s0370-2693(02)01735-5
131. Pilaftsis A, Underwood TEJ. Electroweak-scale resonant leptogenesis. *Phys Rev D* (2005) 72:113001. [hep-ph/0506107]. doi:10.1103/physrevd.72.113001
132. Chun EJ, Cvetic G, Dev PSB, Drewes M, Fong CS, Garbrecht B et al. Probing leptogenesis. *Int J Mod Phys A* (2018) 33(1842005). [1711.02865]. doi:10.1142/s0217751x18420058
133. Dodelson S, Widrow LM. Sterile-neutrinos as dark matter. *Phys Rev Lett* (1994) 72:17–20. [hep-ph/9303287]. doi:10.1103/physrevlett.72.17
134. Drewes M, Adhikari R, Agostini M, Anh Ky N, Araki T, Archidiacono M et al. A white paper on keV sterile neutrino dark matter. *JCAP* (2017) 01:025. 1602.04816.
135. Boyarsky A, Drewes M, Lasserre T, Mertens S, Ruchayskiy O. Sterile neutrino dark matter. *Prog Part Nucl Phys* (2019) 104:1–45. [1807.07938]. doi:10.1016/j.pnpnp.2018.07.004
136. Shi X-D, Fuller GM. New dark matter candidate: Nonthermal sterile neutrinos. *Phys Rev Lett* (1999) 82:2832–5. [astro-ph/9810076]. doi:10.1103/physrevlett.82.2832
137. Laine M, Shaposhnikov M. Sterile neutrino dark matter as a consequence of nuMSM-induced lepton asymmetry. *JCAP* (2008) 06(031). 0804.4543.
138. Ghiglieri J, Laine M. Improved determination of sterile neutrino dark matter spectrum. *JHEP* (2015) 11171. [1506.06752].
139. Venumadhav T, Cyr-Racine F-Y, Abazajian KN, Hirata CM. Sterile neutrino dark matter: Weak interactions in the strong coupling epoch. *Phys Rev D* (2016) 94:043515. [1507.06655]. doi:10.1103/physrevd.94.043515
140. Shaposhnikov M. The nuMSM, leptonic asymmetries, and properties of singlet fermions. *JHEP* (2008) 08008. 0804.4542.
141. Canetti L, Drewes M, Shaposhnikov M. Sterile neutrinos as the origin of dark and baryonic matter. *Phys Rev Lett* (2013) 110:061801. [1204.3902]. doi:10.1103/physrevlett.110.061801
142. Canetti L, Drewes M, Frossard T, Shaposhnikov M. Dark matter, baryogenesis and neutrino oscillations from right handed neutrinos. *Phys Rev D* (2013) 87:093006. [1208.4607]. doi:10.1103/physrevd.87.093006

143. Ghiglieri J, Laine M. Sterile neutrino dark matter via coinciding resonances. *JCAP* (2020) 07(012). 2004.10766.
144. Kusenko A, Takahashi F, Yanagida TT. Dark matter from split seesaw. *Phys Lett B* (2010) 693:144–8. [1006.1731]. doi:10.1016/j.physletb.2010.08.031
145. Li T, Chao W. Neutrino masses, dark matter and symmetry at the LHC. *Nucl Phys B* (2011) 843:396–412. [1004.0296]. doi:10.1016/j.nuclphysb.2010.10.004
146. Escudero M, Rius N, Sanz V. Sterile neutrino portal to Dark Matter I: The $U(1)_{B-L}$ case. *JHEP* (2017) 02:045. 1606.01258.
147. Bezrukov F, Hettmansperger H, Lindner M. keV sterile neutrino Dark Matter in gauge extensions of the Standard Model. *Phys Rev D* (2010) 81:085032. [0912.4415]. doi:10.1103/physrevd.81.085032
148. Bezrukov F, Kartavtsev A, Lindner M. Leptogenesis in models with keV sterile neutrino dark matter. *J Phys G: Nucl Part Phys* (2013) 40:095202. [1204.5477]. doi:10.1088/0954-3899/40/9/095202
149. Nemevsek M, Senjanovic G, Zhang Y. Warm dark matter in low scale left-right theory. *JCAP* (2012) 07:006. 1205.0844.
150. Shaposhnikov M, Tkachev I. The vMSM, inflation, and dark matter. *Phys Lett B* (2006) 639:414–7. [hep-ph/0604236]. doi:10.1016/j.physletb.2006.06.063
151. Petraki K, Kusenko A. Dark-matter sterile neutrinos in models with a gauge singlet in the Higgs sector. *Phys Rev D* (2008) 77:065014. [0711.4646]. doi:10.1103/physrevd.77.065014
152. Boyanovsky D. Clustering properties of a sterile neutrino dark matter candidate. *Phys Rev D* (2008) 78:103505. [0807.0646]. doi:10.1103/physrevd.78.103505
153. Frigerio M, Yaguna CE. Sterile neutrino dark matter and low scale leptogenesis from a charged scalar. *Eur Phys J C* (2015) 75(31). [1409.0659]. doi:10.1140/epjc/s10052-014-3252-1
154. Drewes M, Kang JU. Sterile neutrino Dark Matter production from scalar decay in a thermal bath. *JHEP* (2016) 05(051). [1510.05646].
155. Merle A, Niro V, Schmidt D. New production mechanism for keV sterile neutrino dark matter by decays of frozen-in scalars. *JCAP* (2014) 03028. 1306.3996.
156. König J, Merle A, Totzauer M. keV sterile neutrino dark matter from singlet scalar decays: The most general case. *JCAP* (2016) 11:038. [1609.01289].
157. Peccei RD, Quinn HR. CPConservation in the presence of pseudoparticles. *Phys Rev Lett* (1977) 38:1440–3. doi:10.1103/physrevlett.38.1440
158. Peccei RD, Quinn HR. Constraints imposed by CPConservation in the presence of pseudoparticles. *Phys Rev D* (1977) 16:1791–7. doi:10.1103/physrevd.16.1791
159. Weinberg S. A new light boson? *Phys Rev Lett* (1978) 40:223–6. doi:10.1103/physrevlett.40.223
160. Wilczek F. Problem of StrongPantInvariance in the presence of instantons. *Phys Rev Lett* (1978) 40:279–82. doi:10.1103/physrevlett.40.279
161. Preskill J, Wise MB, Wilczek F. Cosmology of the invisible axion. *Phys Lett B* (1983) 120:127–32. doi:10.1016/0370-2693(83)90637-8
162. Dine M, Fischler W. The not so harmless axion. *Phys Lett B* (1983) 120:137–41. doi:10.1016/0370-2693(83)90639-1
163. Kamionkowski M, March-Russell J. Planck scale physics and the Peccei-Quinn mechanism. *Phys Lett B* (1992) 282:137–41. [hep-th/9202003]. doi:10.1016/0370-2693(92)90492-m
164. Barr SM, Seckel D. Planck scale corrections to axion models. *Phys Rev D* (1992) 46:539–49. doi:10.1103/physrevd.46.539
165. Holman R, Hsu SDH, Kephart TW, Kolb EW, Watkins R, Widrow LM. Solutions to the strong CP problem in a world with gravity. *Phys Lett B* (1992) 282:132–6. [hep-ph/9203206]. doi:10.1016/0370-2693(92)90491-1
166. Ghigna S, Lusignoli M, Roncadelli M. Instability of the invisible axion. *Phys Lett B* (1992) 283:278–81. doi:10.1016/0370-2693(92)90019-z
167. Rubakov VA. Grand unification and heavy axion. *JETP Lett* (1997) 65:621–4. [hep-ph/9703409]. doi:10.1134/1.567390
168. Holdom B, Peskin ME. Raising the axion mass. *Nucl Phys B* (1982) 208:397–412. doi:10.1016/0550-3213(82)90228-0
169. Berezhiani Z, Gianfagna L, Giannotti M. Strong CP problem and mirror world: The Weinberg-Wilczek axion revisited. *Phys Lett B* (2001) 500:286–96. [hep-ph/0009290]. doi:10.1016/s0370-2693(00)01392-7
170. Hook A. Anomalous solutions to the StrongCPProblem. *Phys Rev Lett* (2015) 114:141801. [1411.3325]. doi:10.1103/physrevlett.114.141801
171. Fukuda H, Harigaya K, Ibe M, Yanagida TT. Model of visible QCD axion. *Phys Rev D* (2015) 92:015021. [1504.06084]. doi:10.1103/physrevd.92.015021
172. Gherghetta T, Nagata N, Shifman M. A visible QCD axion from an enlarged color group. *Phys Rev D* (2016) 93(115010). [1604.01127]. doi:10.1103/physrevd.93.115010
173. Dimopoulos S, Hook A, Huang J, Marques-Tavares G. A collider observable QCD axion. *JHEP* (2016) 11(052). [1606.03097].
174. Agrawal P, Howe K. Factoring the strong CP problem. *JHEP* (2018) 12(029). [1710.04213].
175. Gaillard MK, Gavela MB, Houtz R, Quilez P, Del Rey R. Color unified dynamical axion. *Eur Phys J C* (2018) 78(972). [1805.06465]. doi:10.1140/epjc/s10052-018-6396-6
176. Nelson AE, Seiberg N. R symmetry breaking versus supersymmetry breaking. *Nucl Phys B* (1994) 416:46–62. [hep-ph/9309299]. doi:10.1016/0550-3213(94)90577-0
177. Goh H-S, Ibe M. R-axion detection at LHC. *JHEP* (2009) 03:049. 0810.5773.
178. Bellazzini B, Mariotti A, Redigolo D, Sala F, Serra J. R-axion at colliders. *Phys Rev Lett* (2017) 119:141804. [1702.02152]. doi:10.1103/physrevlett.119.141804
179. Gripaos B, Pomarol A, Riva F, Serra J. Beyond the minimal composite Higgs model. *JHEP* (2009) 04:070. 0902.1483.
180. Ferretti G, Karateev D. Fermionic UV completions of Composite Higgs models. *JHEP* (2014) 03077. [1312.5330].
181. Belyaev A, Cacciapaglia G, Cai H, Flacke T, Parolini A, Seródio H. Singlets in composite Higgs models in light of the LHC 750 GeV diphoton excess. *Phys Rev D* (2016) 015004. [1512.07242].
182. Ferretti G. Gauge theories of partial compositeness: Scenarios for run-II of the LHC. *JHEP* (2016) 06:107. 1604.06467.
183. Jeong KS, Jung TH, Shin CS. Axionic electroweak baryogenesis. *Phys Lett B* (2019) 790:326–31. [1806.02591]. doi:10.1016/j.physletb.2019.01.036
184. Yue C-X, Zhang H-Y, Wang H. Production of axion-like particles via vector boson fusion at future electron-positron colliders. *Eur Phys J C* (2022) 82(88). [2112.11604]. doi:10.1140/epjc/s10052-022-10007-7
185. Zhang H-Y, Yue C-X, Guo Y-C, Yang S. Searching for axionlike particles at future electron-positron colliders. *Phys Rev D* (2021) 104:096008. [2103.05218]. doi:10.1103/physrevd.104.096008
186. Coelho RO, Goncalves VP, Martins DE, Rangel MS. Production of axionlike particles in PbPb collisions at the LHC, HE-LHC and FCC: A phenomenological analysis. *Phys Lett B* (2020) 806:135512. 2002.135512. doi:10.1016/j.physletb.2020.135512
187. Bauer M, Neubert M, Thamm A. Collider probes of axion-like particles. *JHEP* (2017) 12:044. 1708.00443.
188. Bauer M, Heiles M, Neubert M, Thamm A. Axion-like particles at future colliders. *Eur Phys J C* (2019) 79:74. 1808.74. doi:10.1140/epjc/s10052-019-6587-9
189. Cacciapaglia G, Deandrea A, Iyer AM, Sridhar K. Tera-Z stage at future colliders and light composite axionlike particles. *Phys Rev D* (2022) 105:015020. [2104.11064]. doi:10.1103/physrevd.105.015020
190. Spira M, Djouadi A, Graudenz D, Zerwas PM. Higgs boson production at the LHC. *Nucl Phys B* (1995) 453:17–82. [hep-ph/9504378]. doi:10.1016/0550-3213(95)00379-7
191. Bauer M, Neubert M, Renner S, Schnubel M, Thamm A. The low-energy effective theory of axions and ALPs. *JHEP* (2021) 04:063. 2012.12272.
192. Knapen S, Thamm A. Direct discovery of new light states at the FCCee. *Eur Phys J Plus* (2021) 136:936. 2108.08949. doi:10.1140/epjp/s13360-021-01874-2
193. Schäfer R, Tillinger F, Westhoff S. Near or far detectors? Optimizing long-lived particle searches at electron-positron colliders, 2202.11714.
194. Tian M, Wang K, Wang ZS. Search for long-lived axions with far detectors at future lepton colliders, 2201.08960.
195. Fruguele C, Fuchs E, Perez G, Schlaffer M. Relaxion and light (pseudo) scalars at the HL-LHC and lepton colliders. *JHEP* (2018) 10:151. 1807.10842.
196. de Blas J, Ciuchini M, Franco E, Mishima S, Pierini M, Reina L et al. Electroweak precision observables and Higgs-boson signal strengths in the standard model and beyond: Present and future. *JHEP* (2016) 12(135). [1608.01509].
197. de Blas J, Cepeda M, D'Hondt J, Ellis RK, Grojean C, Heinemann B et al. *Higgs Boson Studies at Future Particle Colliders*, 01139 (2020). 1905.03764.JHEP.
198. Cepeda M, Gori S, Outschoorn VM, Shelton J *Exotic Higgs Decays*, 2111. p. 12751.

199. Alipour-Fard S, Craig N, Jiang M, Koren S. Long live the Higgs factory: Higgs decays to long-lived particles at future lepton colliders. *Chin Phys C* (2019) 43: 053101. [1812.05588]. doi:10.1088/1674-1137/43/5/053101
200. Strassler MJ, Zurek KM. Echoes of a hidden valley at hadron colliders. *Phys Lett B* (2007) 651:374–9. [hep-ph/0604261]. doi:10.1016/j.physletb.2007.06.055
201. Strassler MJ, Zurek KM. Discovering the Higgs through highly-displaced vertices. *Phys Lett B* (2008) 661:263–7. [hep-ph/0605193]. doi:10.1016/j.physletb.2008.02.008
202. Han T, Si Z, Zurek KM, Strassler MJ. Phenomenology of hidden valleys at hadron colliders. *JHEP* (2008) 07:008. [0712.2041].
203. Chacko Z, Goh H-S, Harnik R. The Twin Higgs: Natural electroweak breaking from mirror symmetry. *Phys Rev Lett* (2006) 96:231802. [hep-ph/0506256]. doi:10.1103/physrevlett.96.231802
204. Burdman G, Chacko Z, Goh H-S, Harnik R. Folded supersymmetry and the LEP paradox. *JHEP* (2007) 02:009. [hep-ph/0609152].
205. Cai H, Cheng H-C, Terning J. A quirky little Higgs model. *JHEP* (2009) 05: 045. 0812.0843.
206. Craig N, Katz A, Strassler M, Sundrum R. Naturalness in the dark at the LHC. *JHEP* (2015) 07:105. [1501.05310].
207. Curtin D, Essig R, Gori S, Jaiswal P, Katz A, Liu T et al. Exotic decays of the 125 GeV Higgs boson. *Phys Rev D* (2014) 90:075004. [1312.4992]. doi:10.1103/physrevd.90.075004
208. Haisch U, Kamenik JF, Malinauskas A, Spira M. Collider constraints on light pseudoscalars. *JHEP* (2018) 03:178. 1802.02156.
209. Fuchs E, Matsedonskiy O, Savoray I, Schlaffer M. Collider searches for scalar singlets across lifetimes. *JHEP* (2021) 04:019. 2008.12773.
210. Cui Y, Shuve B. Probing baryogenesis with displaced vertices at the LHC. *JHEP* (2015) 02:049. 1409.6729.
211. Batell B, Pospelov M, Shuve B. Shedding light on neutrino masses with dark forces. *JHEP* (2016) 08:052. 1604.06099.
212. Accomando E, Delle Rose L, Moretti S, Olaiya E, Shepherd-Themistocleous CH. Novel SM-like Higgs decay into displaced heavy neutrino pairs in $U(1)'$ models. *JHEP* (2017) 04:081. 1612.05977.
213. Accomando E, Delle Rose L, Moretti S, Olaiya E, Shepherd-Themistocleous CH. Extra Higgs boson and Z' as portals to signatures of heavy neutrinos at the LHC. *JHEP* (2018) 02:109. 1708.03650.
214. Curtin D, Essig R, Gori S, Shelton J. Illuminating dark photons with high-energy colliders. *JHEP* (2015) 02157. [1412.0018].
215. Stelzer T, Long WF. Automatic generation of tree level helicity amplitudes. *Comput Phys Commun* (1994) 81:357–71. [hep-ph/9401258]. doi:10.1016/0010-4655(94)90084-1
216. Alwall J, Frederix R, Frixione S, Hirschi V, Maltoni F, Mattelaer O et al. The automated computation of tree-level and next-to-leading order differential cross sections, and their matching to parton shower simulations. *JHEP* (2014) 07(079). [1405.0301].
217. Sjöstrand T, Ask S, Christiansen JR, Corke R, Desai N, Ilten P et al. An introduction to PYTHIA 8.2. *Comput Phys Commun* (2015) 191(159)–77. [1410.3012]. doi:10.1016/j.cpc.2015.01.024
218. DELPHES 3 collaboration, de Favereau J, Delaere C, Demin P, Giammanco A, Lemaitre V, Mertens A et al. DELPHES 3, A modular framework for fast simulation of a generic collider experiment. *JHEP* (2014) 02:057. 1307.6346.
219. collaboration, Antonello M. Idea: A detector concept for future leptonic colliders. *Nuovo Cim C* (2020) 43:27.
220. Volkl V, Madlener T, Helsens C, key4hep/k4simdelphes: v00-01-07, 2021. doi:10.5281/zenodo.5585287
221. Volkl V, Madlener T, Gaede F, Sailer A, Helsens C, Declara PF et al. key4hep/edm4hep: v00-04, 2021. doi:10.5281/zenodo.5585967
222. Guiraud E, Naumann A, Piparo D. *Tdataframe: Functional chains for root data analyses* (2017). doi:10.5281/zenodo.260230
223. Brun R, *root-project/root: v6.18/02*, 2019. doi:10.5281/zenodo.3895860
224. Ai X, Allaire C, Calace N, Gessinger P, Grasland H, Gray H et al. Acts project: v8.3.0, 2021. doi:10.5281/zenodo.4818137
225. Cacciari M, Salam GP, Soyez G. FastJet user manual. *Eur Phys J C* (2012) 72: 1896. [1111.6097]. doi:10.1140/epjc/s10052-012-1896-2
226. Pivarski J, Osborne I, Das P, Hollands A, Schreiner H, Biswas A et al. scikit-hep/awkward-1.0: 1.8.0rc3, 2022. doi:10.5281/zenodo.5885291
227. Alva D, Han T, Ruiz R. *Heavy Majorana neutrinos from W γ fusion at hadron colliders*. *JHEP* (2015) 02:072. [1411.7305].
228. Degrande C, Mattelaer O, Ruiz R, Turner J. Fully-Automated precision predictions for heavy neutrino production mechanisms at hadron colliders. *Phys Rev D* (2016) 94:053002. [1602.06957]. doi:10.1103/physrevd.94.053002
229. Christensen ND, Duhr C. FeynRules - Feynman rules made easy. *Comput Phys Commun* (2009) 180:1614–41. [0806.4194]. doi:10.1016/j.cpc.2009.02.018
230. Degrande C, Duhr C, Fuks B, Grellscheid D, Mattelaer O, Reiter T. UFO - the universal FeynRules output. *Comput Phys Commun* (2012) 183:1201–14. [1108.2040]. doi:10.1016/j.cpc.2012.01.022
231. Alloul A, Christensen ND, Degrande C, Duhr C, Fuks B. FeynRules 2.0 - a complete toolbox for tree-level phenomenology. *Comput Phys Commun* (2014) 185: 2250–300. [1310.1921]. doi:10.1016/j.cpc.2014.04.012
232. Bacchetta N, Cld - a detector concept for the FCC-ee, (2019) 1911.12230.
233. Ruiz RE. PhD thesis, 1509. Pittsburgh U. (2015). p. 06375. *Hadron Collider Tests of Neutrino Mass-Generating Mechanisms*.